Quaternary Research (2024), **122**, 122–142
doi:10.1017/qua.2024.24

Research Article

Sedimentologic successions and chronology of the late Pleistocene deposits on the southern Kola Peninsula, northern Europe

Olga Korsakova[a,b], Anatoly Molodkov[c], Nataliya Zaretskaya[b,d,e] and Vasily Grigoriev[f]

[a]Geological Institute of the Kola Science Centre of the Russian Academy of Sciences, 184209 Apatity, Russia; [b]VNIIOkeangeologia, 190121 St. Petersburg, Russia; [c]Research Laboratory for Quaternary Geochronology, Department of Geology, Tallinn University of Technology, 19086 Tallinn, Estonia; [d]Institute of Geography, Russian Academy of Sciences, 119017 Moscow, Russia; [e]Geological Institute, Russian Academy of Sciences, 119017 Moscow, Russia and [f]St. Petersburg State University, 199034 St. Petersburg, Russia

Abstract

Late Pleistocene deposits in the southern Kola Peninsula, adjacent to the White Sea, evidence the complex alternation between marine transgressions and glacial expansions in northern Europe during successive late Pleistocene warm and cold stages. According to lithostratigraphic and chronological data from key sections, southern Kola Peninsula underwent two phases of the Boreal marine transgression during Marine Isotope Stage (MIS) 5; marine environments, encompassing the very end of MIS 4 and almost the entirety of MIS 3, were also recognized. Age determinations using electron spin resonance (ESR) and infrared optically stimulated luminescence (IR-OSL) techniques reveal marine sediments with ages ranging from 138–128 ka to 72.4 ± 5.6 ka in the Varzuga, Chavanga, Chapoma 1 and 2, and Bolshaya Kumzhevaya sections, indicating initial and second phases of the Boreal transgression. The presence of marine deposits with ages ranging from ca. 59 ka to 37 ka in the Chavanga, Kamenka, Chapoma 2, and Bolshaya Kumzhevaya sections also suggests an accumulation stage in the marine environment. The research material from the studied sections provides evidence of a short glacier expansion into coastal areas of the White Sea during early MIS 4 and a continuous glaciation from the late MIS 3 and throughout MIS 2.

Keywords: Tersky Coast, Marine transgressions, Glacial expansions, Lithology, Chronometry

(Received 14 December 2023; accepted 24 April 2024)

Introduction

The Kola Peninsula, next to the White and Barents Seas, was subjected to several marine transgressions and glacier expansions during successive late Pleistocene warm and cold stages. In the early Marine Isotope Stage (MIS) 5, huge areas in NW Russia, including valleys and plains of the Kola Peninsula, were flooded by transgressive seas associated with a number of global hydrological, geologic, and climatic processes. The Boreal marine transgression that is identified by many researchers (Lavrova, 1960; Gudina and Yevzerov, 1973; Faustova, 1984; Molodkov and Raukas, 1998; Ikonen and Ekman, 2001; Molodkov and Bolikhovskaya, 2002, 2009; Lunkka et al., 2018; Korsakova, 2021) was the largest in the late Pleistocene history of the Kola Peninsula. It is believed that the Kola region and adjacent White Sea depression were covered by the Scandinavian Ice Sheet (SIS) during the last cold stage (late Valdaian, late Weichselian, MIS 2) (Lavrova, 1960; Ekman and Iljin, 1991; Kleman et al., 1997; Yevzerov, 2001; Svendsen et al., 2004; Demidov et al., 2006; Hättestrand et al., 2007; Hughes at al., 2016; Stroeven et al., 2016; Lunkka et al., 2018; Boyes et al., 2021). These two late Pleistocene events are clearly traced by palaeoenvironmentally controlled sedimentary processes and are relatively well represented in the depositional successions. Details of the Kola region's sedimentary history during the late MIS 5, MIS 4, and MIS 3 periods are more elusive, although the general outlines of the late Pleistocene stratigraphy are established. Known litho-chrono-biostratigraphic data, as well as sedimentary analyses and numerical dating studies and their interpretation, are summarized in Gudina and Yevzerov (1973), Ikonen and Ekman (2001), Molodkov and Bolikhovskaya (2002, 2009), Svendsen et al. (2004), Korsakova (2019, 2021), Hughes et al. (2016), Korsakova et al. (2016), Lunkka et al. (2018), Zaretskaya et al. (2019, 2022), and Boyes et al. (2021, 2023).

However, different opinions still remain concerning the extent and age of the late Pleistocene glacial advances, as well as the number and timing of marine transgressions. Mollusc-bearing clayey mud, silt, and sand containing marine diatoms are known in the fluvial and marine terraces from several localities in coastal Kola Peninsula (Grave et al., 1969; Gudina and Yevzerov, 1973; Ikonen and Ekman, 2001; Molodkov and Yevzerov, 2004; Korsakova et al., 2004, 2016; Korsakova, 2021). Early work by Gudina and Yevzerov (1973) attributed these marine beds to two middle Valdaian (middle Weichselian, MIS 3) transgressions—the relatively warm-water Ponoy transgression and the colder-water Strelna one, represented by so-called Ponoy Beds and Strelna Beds, respectively. Later, the Ponoy transgression was correlated with MIS 5e, and the Strelna transgression with the MIS 3 interglacial period

Corresponding author: Olga Korsakova; Email: korsak@geoksc.apatity.ru

Cite this article: Korsakova O, Molodkov A, Zaretskaya N, Grigoriev V (2024). Sedimentologic successions and chronology of the late Pleistocene deposits on the southern Kola Peninsula, northern Europe. *Quaternary Research* **122**, 122–142. https://doi.org/10.1017/qua.2024.24

(Yevzerov, 1993). On the other hand, based on biostratigraphic data (Lavrova, 1960; Nikonov and Vostrukhina, 1964; Armand and Lebedeva, 1966; Grave et al., 1969; Gudina and Yevzerov, 1973; Strelkov et al., 1976; Ikonen and Ekman, 2001), uranium-thorium (^{230}Th/U), electron spin resonance (ESR), feldspar-based infrared optically stimulated luminescence (IR-OSL) dates, and amino acid ratios (Arslanov et al., 1981; Miller and Mangerud, 1985; Ikonen and Ekman, 2001; Molodkov and Yevzerov, 2004; Korsakova et al., 2004, 2016; Zaretskaya et al., 2019, 2022), it has been concluded that the Ponoy Beds and Strelna Beds were deposited on the Kola Peninsula by two phases of a single marine transgression during the last interglacial, that is, the Mikulinian warming (MIS 5); a third marine unit formed during the MIS 3 warming.

It is considered that at least two late Pleistocene glacial events are represented on the Kola Peninsula, suggesting two separate ice advances (Nikonov, 1966; Armand et al., 1969; Grave et al., 1969; Apukhtin, 1978; Hättestrand et al., 2007; Yevzerov, 2016; Boyes et al., 2021, 2023; Korsakova, 2021) during MIS 5d–MIS 4 and MIS 2. Situated in a coalescing zone of the several ice sheets, Kola Peninsula was generally accepted to be covered by the SIS and Barents Sea Ice Sheet (BSIS) (Grosswald, 2001; Grosswald and Hughes, 2002; Svendsen et al., 2004; Kjær et al., 2006; Lambeck et al., 2006, 2010; Larsen et al., 2006; Stroeven et al, 2016; Korsakova, 2021). However, almost all researchers involved in the glacial geology of European Russia agree that neither the late Valdaian (late Weichselian, MIS 2) BSIS nor the Barents-Kara Ice Sheet advanced into the Kola Peninsula (Ekman and Iljin, 1991; Yevzerov, 2001; Svendsen et al., 2004; Kjær et al., 2006; Larsen et al., 2006; Pasanen et al., 2010; Stroeven et al., 2016; Korsakova et al., 2021), although the BSIS may have reached the Kola Peninsula in MIS 4 (Svendsen et al., 2004; Lambeck et al., 2006; Larsen et al., 2006; Korsakova et al., 2007; Korsakova, 2021).

Later glacial advances and related glacioaqueous erosion considerably destroyed unconsolidated deposits formed before these events. However, they have been preserved quite completely on the southern Kola Peninsula, where they outcrop along riverbanks or in coastal cliffs. Here, lithologic and chronological investigations of sedimentary successions were undertaken to obtain data about the ages, textures, and structure of deposits that would allow the history of the main changes of sedimentary settings to be determined. The primary objectives of this paper are to discuss and evaluate the obtained and available published results, identify the constituent units of the late Pleistocene depositional sequences in the southern Kola Peninsula, and associate them with the main marine and glacial events, as well as to determine the chronology of the main depositional stages. In this contribution, we present new lithostratigraphic observations and chronological data from the series of the key sections in the southern Kola Peninsula that can shed light on the late Pleistocene depositional settings and palaeogeographic events in the European north.

Study Area

The investigated sites are located on the western and southeastern Tersky Coast of the White Sea (Fig. 1). In the southern Kola Peninsula, bedrock is composed of Archaean and Lower and Upper Proterozoic metamorphic gneiss, amphibolite, migmatite, intrusive igneous granodiorite, tonalite, trondhjemite, and metasedimentary arcosic and polimict sandstone and siltstone (Mitrofanov, 2001). The position of the river valleys tends to be predetermined by the neotectonic pattern of the northeastern Fennoscandian Shield, including the Kola Peninsula (Koshechkin, 1979; Strelkov et al., 1976).

Quaternary deposits in the study area are mainly composed of glacial, glaciofluvial, glaciolacustrine, glaciomarine, marine, and aeolian sediments (Astafiev et al., 2012). The main geomorphological features on the Tersky Coast are primary shaped by the last glaciation, with late Valdaian (late Weichselian, MIS 2) tills and various glacial deposits dominating the landscape on the Kola Peninsula. Landforms such as fluting moraine, hummocky moraine, end moraine complexes, glacifluvial and glaciolacustrine toplands, eskers, and glacifluvial deltas have been identified through mapping efforts (Hättestrand and Clark, 2006; Boyes et al., 2021, 2023). Coastal landforms in the late glacial and Holocene are largely composed of marine sediments and are found within a narrow coastal zone. The upper marine limit, which decreases from west to east, has been reconstructed to be approximately 35–40 m above sea level (m asl) and 10–12 m asl in the lower Varzuga and Chapoma Rivers, respectively (Kolka and Korsakova, 2017). Additionally, Holocene aeolian landforms occur in the coastal zone. Some late Pleistocene glacial, glacioaqueous, and marine deposits, though localized, are buried beneath the late Valdaian (late Weichselian, MIS 2) and Holocene sediments.

Key sections with different types of deposits are exposed in the lower reach of the Varzuga, Chavanga, Kamenka, Chapoma, and Bolshaya Kumzhevaya Rivers, which all enter into the White Sea.

Methods

Field investigations

Fieldwork through the Tersky Coast of the White Sea included sedimentologic, lithostratigraphic, and other traditional geologic investigations of the sedimentary sequences in the outcrops, sampling for numerical dating, and unmanned aerial vehicle survey. Sedimentary sequences were sketched in the field and logged with a vertical resolution of 1:50. Sediments were classified according to the size of their components, as follows: (1) boulders: more than 100 mm; (2) pebbles: 10–100 mm; (3) gravel: 1–10 mm; (4) sand: 1.0–0.01 mm; and (5) silt and clay: <0.01 mm. The colour of deposits was identified according to the Munsell Soil Classification System. The samples for IR-OSL dating were collected according to a standard procedure by driving ca. 30-cm-long opaque plastic tubes into a cleaned face of the outcrop, then capping and sealing them to retain moisture. In total, six river and coastal sections were studied (Fig. 1). Elevation above sea level (asl) of the sections and lithostratigraphic units was measured using the 5× magnifying CB-17-630 Berger Hand Level and the Differential Global Positioning System total station.

IR-OSL dating

IR-OSL ages in this paper were obtained at the Research Laboratory for Quaternary Geochronology (RLQG) at Tallinn University of Technology.

The IR-OSL method uses potassium feldspar found in the Earth's crust to date sediments (Huntley et al., 1985; Godfrey-Smith et al., 1988). It relies on trapped charges (electrons) within the crystal structure of feldspar minerals, released

https://doi.org/10.1017/qua.2024.24 Published online by Cambridge University Press

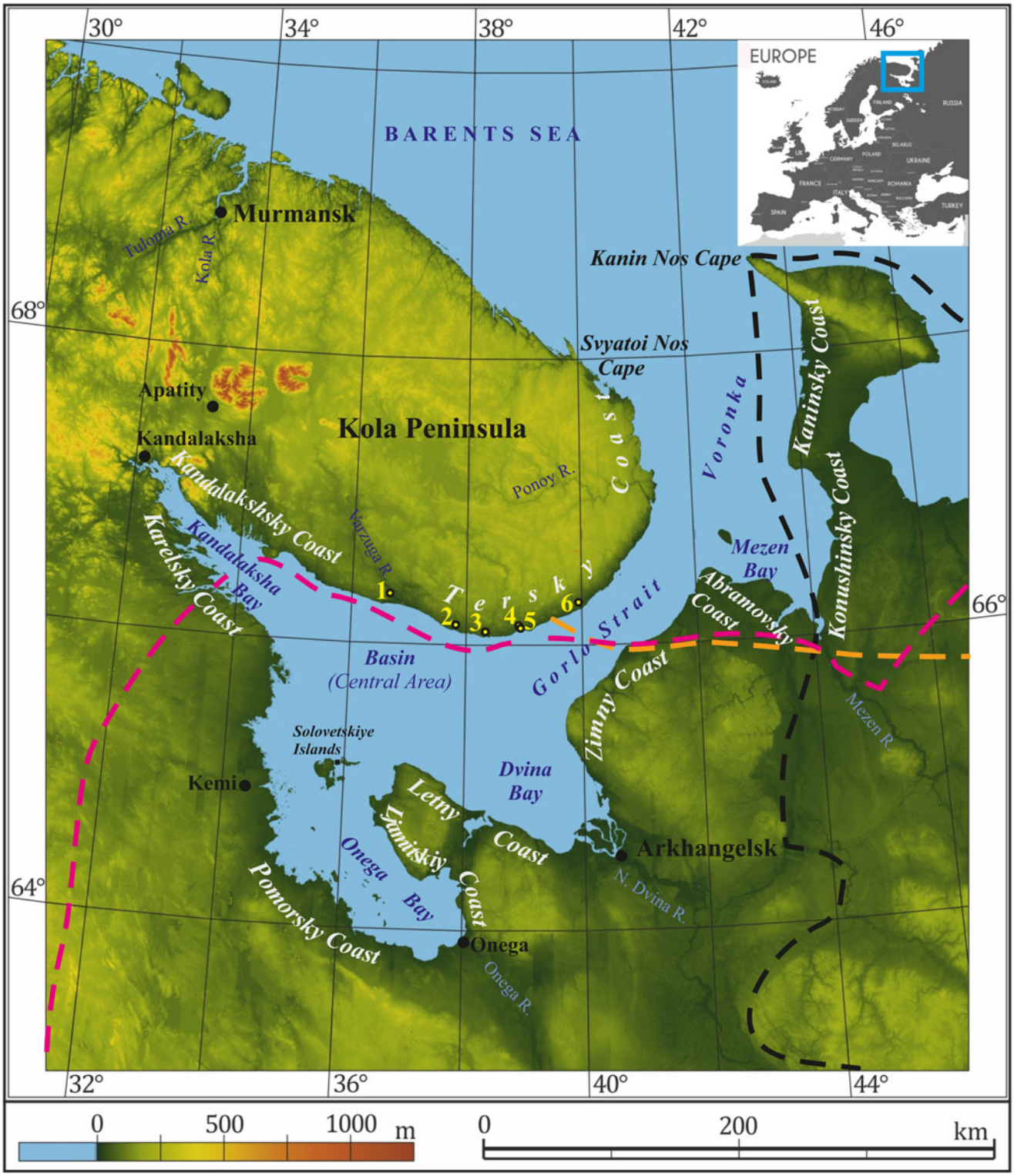

Figure 1. White Sea and location of the key sections: 1, Varzuga; 2, Chavanga; 3, Kamenka; 4, Chapoma 1; 5, Chapoma 2; 6, Bolshaya Kumzhevaya. Dotted coloured lines show glaciation limits during MIS 4 at 60 ka (magenta line; after Svendsen et al., 2004) and at 70–65 ka (orange line; after Larsen et al., 2006) and during the last glacial maximum (LGM) (black line; after Demidov et al., 2006). The insert shows the study area (blue rectangle) on the map of Europe. Digital terrain model by Farr et al. (2007).

when the grains are exposed to infrared radiation in the lab. The brightness of the luminescence signal corresponds to the natural ionizing radiation dose (palaeodose), correlating with the sedimentary age.

To determine a sample's age, accumulated palaeodose (P) and total natural radiation dose rate (D_Σ) are considered. The age-correlating palaeodose has been accumulated in the mineral grains from the time the sedimentary material was last exposed

https://doi.org/10.1017/qua.2024.24 Published online by Cambridge University Press

to daylight, while the total dose rate includes contributions from cosmic radiation, sedimentary matrix, and the decay of ^{40}K within the mineral. Potassium feldspar grains (100–150 μm) were extracted from sediment using a specific procedure (Molodkov and Bitinas, 2006). IR-OSL measurements were conducted at room temperature using a thermoluminescence (TL)/IR-OSL reader.

The dose–response curves were used to determine palaeodose through the multiple-aliquot additive-dose protocol. External beta and gamma contributions to the total dose rate (D_Σ) were estimated in the lab using specific factors (Adamiec and Aitken, 1998). The in situ water content was considered. The contribution of cosmic dose rates to total dose rates was calculated using formulae provided by Prescott and Hutton (1994). The internal beta dose from decay of ^{40}K and ^{87}Rb was obtained based on recommended concentration estimates from Huntley and Baril (1997) and Huntley and Hancock (2001). The K-feldspar samples were not preheated or thermally treated but stored for about 1 month at room temperature to reduce postirradiational phosphorescence (Molodkov and Bitinas, 2006).

^{230}Th/U dating

The ^{230}Th/U dating was performed at the Laboratory for Polar and Marine Research, Earth Science Institute, St.-Petersburg University (Russia) on shell samples (*Arctica islandica*) from the marine deposits. The ^{230}Th/U dating of shells includes the determination of uranium and thorium isotopes either in the whole carbonate skeleton or in its individual parts. The content of uranium and thorium isotopes in the external and internal fractions was quantified using radiochemical techniques (Maximov et al., 2016). Often-observed variance in the distribution of uranium and thorium isotopes between the inner and outer layers of fossil shells can be attributed to their disparate postmortem uptake and migration into mollusc shells from the surrounding environment (Kaufman et al., 1996; Labonne and Hillaire-Marcel, 2000; Maksimov et al., 2016; Ayling et al., 2017). According to the known equation (Kaufman and Broecker, 1965), the ^{230}Th/U age and its error for the corresponding fractions were calculated from the values of activity ratios of thorium and uranium isotopes.

Results

Varzuga section

The Varzuga section is located on the right bank of the Varzuga River, 20 km upstream from its mouth, on the westernmost Tersky Coast (1 in Fig. 1). Here, strong river lateral erosion impacts an elongated hill with an elevation of 53–54 m asl at its peak. Its pitted surface is 15–25 m above adjacent areas. Due to the active slumping, the available sequence varies from year to year. Having been discovered in 1898 (Rippas, 1899), this outcrop, elongated for 2 km along an abrupt slope of the river valley, was subsequently and repeatedly investigated (Apukhtin, 1957; Lavrova, 1960; Armand and Lebedeva, 1966; Nikonov, 1966; Gudina and Yevzerov, 1973; Yevzerov et al., 1981; Korsakova et al., 2004, 2019; Molodkov and Yevzerov, 2004; Lunkka et al., 2018; Zaretskaya et al., 2022).

The late Pleistocene sedimentary succession studied by us lies in the middle part of the Varzuga outcrop (66°23.77′N, 36°39.00′E) at 16–31 m asl, where corresponding deposits are superposed on middle Pleistocene marine and glacial sediments (Korsakova et al., 2019). The sedimentary log is shown in Figure 2 (section 1). The lower part of the studied sequence is composed of dark grayish-brown clay and silty clay, which are dated to 245 ± 27/21 ka by the ^{230}Th/U method (section 1 in Fig. 2, Table 1). The late Pleistocene sequence begins with dark gray-brownish compact gravelly clayey silt, silt, and sand that occurred at 16.0–19.9 m asl; an IR-OSL date of 92.8 ± 14.4 ka was obtained from a sandy lens located 1.1 m above the lower contact of this unit. At 19.9–26.5 m asl, this depositional unit is overlain with an erosional contact by an alternation of yellow, olive-yellow, or gray, laminated, solid, fine-grained sand and sandy silt, which are horizontally, ripple-, wavy-, or cross-bedded, deformed upward with microlags, folds, streaked-out ripples, and fine silty partings similar to flames. The two IR-OSL dates of 69.5 ± 5.5 and 66.5 ± 7.9 ka were obtained from this unit at 22.6 and 25.5 m asl, respectively (Zaretskaya et al., 2022; 1 in Fig. 2, Table 1). At 26.5–31.0 m asl in the studied sequence, there is a solid matrix-supported massive diamicton represented by reddish-brown clayey silt with gravel, pebbles, and boulders; its lower contact is sharp and even. The top of the Varzuga section is represented by light brownish-gray medium and fine sand with intercalations of gravel and pebbles.

Chavanga section

The Chavanga section (66°9.03′N, 37°47.13′E) is located on the southern Tersky Coast at an altitude of 28–37 m asl on the right bank of the Chavanga River, 4.1 km from its mouth (2 in Fig. 1).

In the sedimentary succession (2 in Fig. 2), gray compact silty mud was identified near the river water level at 28.5–29.0 m asl. At 29.0–30.9 (32.0) m asl, it is sharply overlain by coarse sand with gravel and well-rounded flattened pebbles. This unit is sharply overlain with very uneven contact by fine- to medium-grained yellowish sand including small lenses of pinkish-gray sand with fine horizontal lamination and ripple marks: there are pockets and interbeds of fine, medium, and coarse sand at the interval of ca. 30.9 (32.0) to 32.0 (32.4) m asl. The sand at 31.2–31.3 m asl is IR-OSL dated to 53.5 ± 4.1 ka (RLQG 2610-069) (Zaretskaya et al., 2022; 2 in Fig. 2, Table 1). At ca. 32.0 (32.4) to 35.9 m asl, yellowish-brown sand with indistinct lamination and spots of grayish sand and lenses of sandy silt, probably glaciotectonically deformed, occurs; IR-OSL dates show these deposits accumulated no earlier than 18.4–17.8 ka (Zaretskaya et al., 2022; 2 in Fig. 2). At the top of the sequence, compact poorly sorted sandy and clayey silt with gravel, pebbles, and small boulders occurs at 35.9–36.2 m asl and is overlain with trough-shaped contact by poorly sorted sand with gravel at the interval of 36.2–37.0 m asl.

Kamenka section

The Kamenka section (66°5.83′N, 38°16.65′E) is located at an altitude of 44–46 m asl on the abrupt right bank of the Kamenka River valley, 4.7 km from its mouth (3 in Fig. 1).

The basal part of the sediment succession (3 in Fig. 2) consists of dark grayish-brown silty clay with boulders up to 30–40 cm in diameter, abundant pebbles, and gravel; local fissility appears as indistinct horizontal thin partings, that is, the diamict splits into numerous lens-shaped plates, a few millimetres to one or

https://doi.org/10.1017/qua.2024.24 Published online by Cambridge University Press

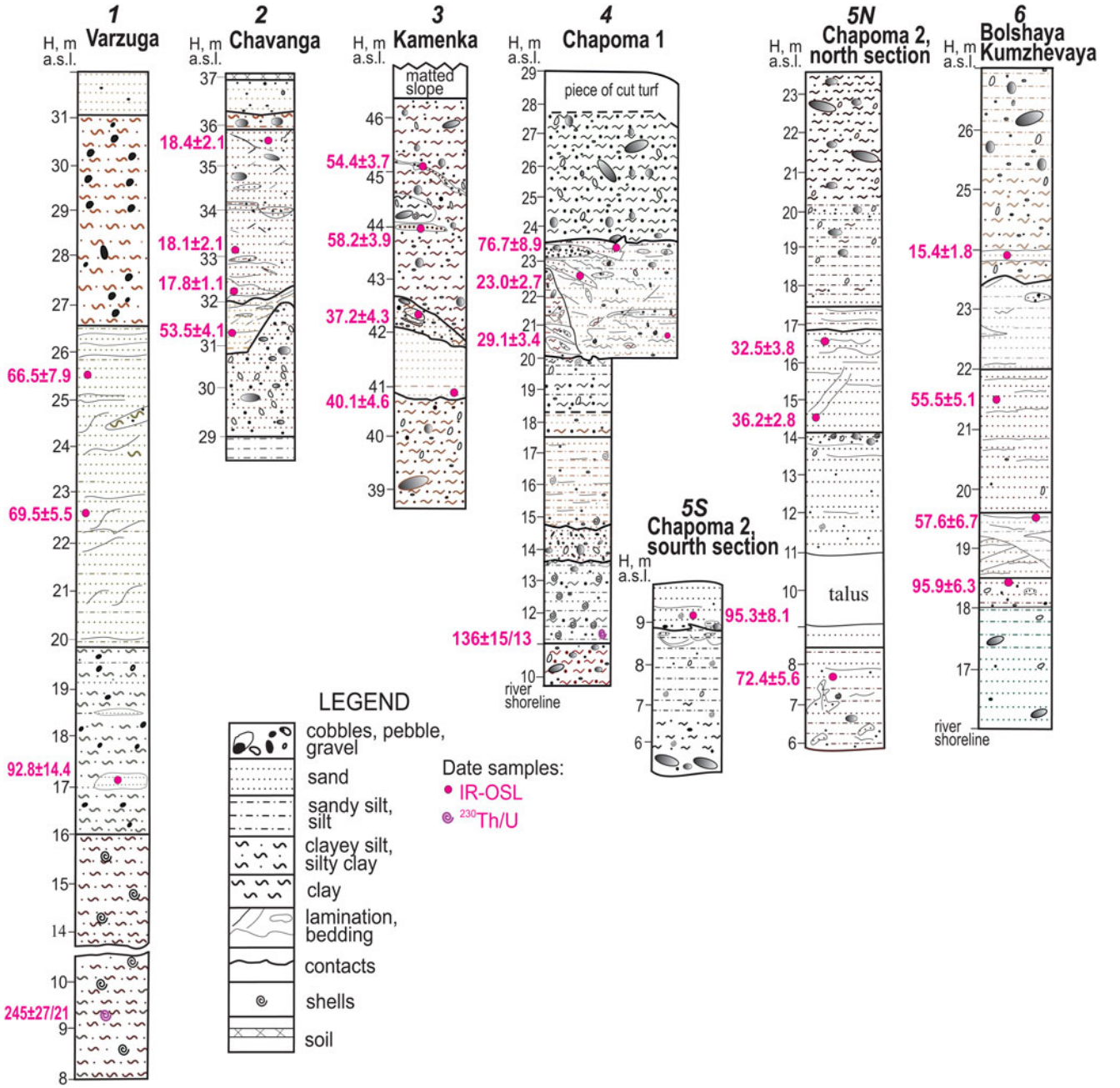

Figure 2. Sediment logs from the studied outcrops. The locations of the sections are shown in Fig. 1.

few centimetres thick. Light brownish-gray fine sand and silt with sharp uneven contact at 40.8–40.9 m asl lies immediately on the clayey sediments; ferruginous rust stains and dark-gray smudges are common for the sand. The IR-OSL method has yielded the age of fine sand and silt to be 40.1 ± 4.6 ka (RLQG 2611-079) (3 in Fig. 2, Table 1). Overlying the fine sand is a lens-shaped unit composed of brown very fine sand with abundant gravel. A pocket of washed fine sand IR-OSL dated to 37.2 ± 4.3 ka (RLQG 2612-079) (3 in Fig. 2, Table 1) occurs at 41.8–42.6 m asl. At 42.6–46.5 m asl, dark-brown silty clay with abundant boulders, pebbles, and gravel was exposed; sandy lenses and streaks are common in this unit. The upper silty clay is moist and massive with gritty texture; included gravel and pebbles are well-rounded and evenly distributed, and some are eroded. Hair-like inclusions similar to aquatic plant remains are visible in these sediments. At 44.0 m asl, a streak of reddish-brown, poorly sorted, predominantly medium sand occurred and is dated to 58.2 ± 3.9 ka (RLQG 2662-070). A pocket of greenish-black silty clay with broken shells and well-rounded small boulders, pebbles, and gravel overlies the lens-shaped sandy texture. A reddish-dark brown sand–gravel–pebble streak of 3–15 cm depth occurs at 44.6–45.1 m asl. These sediments are IR-OSL dated to 54.4 ± 3.7 ka (RLQG 2663-070) (3 in Fig. 2, Table 1). The IR-OSL-dated sandy streaks are suggested to be inclusions in the clayey unit, which occurs at 42.6–46.5 m asl (3 in Fig. 2). Above the streak up to the top, dark-brown silty clay with abundant boulders, pebbles, and gravel is represented in the investigated sequence.

https://doi.org/10.1017/qua.2024.24 Published online by Cambridge University Press

Table 1. Dating results of the Pleistocene deposits from the northern White Sea coast.

Lab no.	Sampling site coordinates[a]	Sampling altitude (m asl)	Dating method	Age (ka)	Palaeodose (*P*) (Gy)	U (ppm)	Th (ppm)	K (%)	References
Varzuga									
RLQG 406-039	66°23.77′N, 36°38.98′E	6.2–6.4	ESR	319.0 ± 38.5	731.0 ± 73.0	1.74	9.44	2.48	Korsakova et al., 2019
RLQG 404-039	66°23.75′N, 36°39.05′E	11.0–11.3	ESR	319.0 ± 22.7	658.7 ± 13.2	2.19	8.07	2.23	Korsakova et al., 2019
RLQG 407-039	66°23.77′N, 36°38.98′E	12.0–12.1	ESR	316.0 ± 23.6	644.0 ± 19.0	2.16	7.91	2.31	Korsakova et al., 2019
LU-557b	66°23.77′N, 36°39.00′′E	9.0–9.2	^{230}Th/U	≥245 ± 27/21					This paper
RLQG 309-042 – RLQG 312-042	66°23.81′N, 37°13.88′E	25.4–25.7	ESR	103.0 ± 4.2	297.7 ± 18.0	1.50	8.73	2.22	Korsakova et al., 2004; Molodkov and Yevzerov, 2004
RLQG 1405-031	66°23.82′N, 37°13.88′E	25.4–25.7	IR-OSL	104.0 ± 8.3	297.7 ± 18.0	1.50	8.73	22.2	Molodkov and Yevzerov, 2004
RLQG 1863-039	66°23.77′N, 36°38.98′E	18.9–19.1	IR-OSL	95.9 ± 11.1	323.6 ± 16.2	1.30	5.24	2.15	Korsakova et al., 2019
RLQG 2664-070	66°23.77′N, 36°39.00′E	17.1–17.2	IR-OSL	92.8 ± 14.4	429.4 ± 61.4	1.28	2.20	3.25	This paper
Risø 993216	66°23.79′N, 36°38.94′E	21.0–21.4	OSL	88 ± 7.0	213 ± 12				Lunkka et al., 2018
Risø 993217	66°23.79′N, 66°38.94′E	29.8–30.0	OSL	70 ± 8.0	165 ± 16				the same
RLQG 2613-079	66°23.77′N, 36°39.00′E	22.6–22.7	IR-OSL	69.5 ± 5.5	233.1 ± 11.7	0.93	4.01	2.19	Zaretskaya et al., 2022
RLQG 2614-079	66°23.77′N, 36°39.00′E	25.5–25.6	IR-OSL	66.5 ± 7.9	242.0 ± 24.0	1.00	3.71	2.33	Zaretskaya et al., 2022
Risø 993218	66°23.79′N, 36°38.94′E	39.1–39.4	OSL	6.2 ± 0.8	28 ± 3				Lunkka et al., 2018
Chavanga									
RLQG 343-073	66°20.03′N, 37°46.85′E	28.5	ESR	99.0 ± 7.6	170.3 ± 15.3	1.53	7.87	2.04	Korsakova et al., 2004
RLQG 1518-103	66°9.03′N, 37°46.91′E	33.0	IR-OSL	63.6 ± 8.0	204.9 ± 22.6	0.62	4.15	2.13	Korsakova et al., 2004
RLQG 2610-069	66°9.03′N, 37°47.13′E	31.2–31.3	IR-OSL	53.5 ± 4.1	159.5 ± 8.0	0.93	4.61	1.72	Zaretskaya et al., 2022
RLQG 2608-069	66°9.03′N, 37°47.13′E	35.7–35.8	IR-OSL	18.4 ± 2.1	55.1 ± 5.1	0.44	2.78	2.78	Zaretskaya et al., 2022

(*Continued*)

Table 1. (*Continued.*)

Lab no.	Sampling site coordinates[a]	Sampling altitude (m asl)	Dating method	Age (ka)	Palaeodose (*P*) (Gy)	U (ppm)	Th (ppm)	K (%)	References
RLQG 2609-069	66°9.03′N, 37°47.13′E	33.1–33.2	IR-OSL	18.1 ± 2.1	53.4 ± 5.3	0.78	5.22	1.61	Zaretskaya et al., 2022
RLQG 2659-070	66°9.03′N, 37°47.13′E	32.3–32.4	IR-OSL	17.8 ± 1.1	51.3 ± 1.3	0.81	3.78	1.65	Zaretskaya et al., 2022
Kamenka									
RLQG 344-073	66°5.68′N, 38°17.17′E	36.5	ESR	58.7 ± 4.4	109.6 ± 3.3	1.57	8.67	2.32	Korsakova et al., 2004
RLQG 2662-070	66°5.83′N, 38°16.65′E	43.9–44.0	IR-OSL	58.2 ± 3.9	218.7 ± 6.6	1.29	8.02	2.20	This paper
RLQG 2663-070	66°5.83′N, 38°16.65′E	44.7–44.8	IR-OSL	54.4 ± 3.7	217.7 ± 6.5	1.60	6.40	2.37	This paper
RLQG 416-119	—	ca. 37.5	ESR	52.0 ± 4.3	124.4 ± 5.0	1.71	9.48	2.46	Astafiev et al., 2012; Korsakova, 2021
RLQG 2611-079	66°5.83′N, 38°16.65′E	40.9–41.0	IR-OSL	40.1 ± 4.6	100.5 ± 10.0	0.42	2.97	1.47	This paper
RLQG 2612-079	66°5.83′N, 38°16.65′E	42.2–42.3	IR-OSL	37.2 ± 4.3	94.3 ± 9.4	0.55	2.50	1.49	This paper
Chapoma 1									
RLQG 395-039B	66°23.82′N, 37°13.88′E	ca. 11.2	ESR	137.0 ± 9.6	146.9 ± 3.0	0.99	3.13	1.45	Molodkov, 2012
LU-479b	66°6.93′N, 38°51.92′E	11.05–11.1	^{230}Th/U	136 ± 15/13					This paper
RLQG 395-039A	66°23.82′N, 37°13.88′E	ca. 11.2	ESR	134.5 ± 9.5	119.9 ± 2.5	0.99	3.13	1.45	Molodkov, 2012
RLQG 267-129	66°23.82′N, 37°13.88′E	ca. 11.4	ESR	126.2 ± 10.1	186.7 ± 3.0	1.15	3.49	1.34	Molodkov and Bolikhovskaya, 2002
LU-464		ca. 12.7	^{230}Th/U	86.0 ± 3.9					Arslanov et al., 1981
RLQG 2601-069	66°6.93′N, 38°51.92′E	23.4–23.5	IR-OSL	76.7 ± 5.9	200.0 ± 10.0	0.53	1.69	1.55	This paper
RLQG 2599-069	66°6.93′N, 38°51.92′E	20.5–20.6	IR-OSL	29.1 ± 3.4	85.5 ± 8.6	0.72	1.82	1.87	This paper
RLQG 2600-069	66°6.93′N, 38°51.92′E	22.3–22.4	IR-OSL	23.0 ± 2.7	65.8 ± 6.6	0.78	1.31	1.80	This paper
Chapoma 2									
RLQG 2661-070	66°6.22′N, 38°53.18′E	9.1–9.2	IR-OSL	95.3 ± 8.1	292.0 ± 17.5	1.12	2.57	1.67	Zaretskaya et al., 2022
RLQG 2604-069	66°6.22′N, 38°53.18′E	7.6–7.7	IR-OSL	72.4 ± 5.6	208.2 ± 10.4	1.05	3.12	1.73	Zaretskaya et al., 2022

RLQG 2603-069	66°6.22′N, 38°53.18′E	14.3–14.4	IR-OSL	36.2 ± 2.8	103.5 ± 5.2	0.47	2.13	1.82	Zaretskaya et al., 2022
RLQG 2602-069	66°6.22′N, 38°53.18′E	16.5–16.6	IR-OSL	32.5 ± 3.8	93.5 ± 9.4	0.30	1.75	1.75	Zaretskaya et al., 2022
Bolshaya Kumzhevaya									
RLQG 2660-070	66°13.60′N, 39°40.48′E	18.3–18.4	IR-OSL	95.9 ± 6.3	266.1 ± 8.0	0.96	2.99	1.68	This paper
RLQG 2607-069	66°13.60′N, 39°40.48′E	19.4–19.5	IR-OSL	57.6 ± 6.7	157.2 ± 7.9	0.45	1.97	1.70	This paper
RLQG 2606-069	66°13.60′N, 39°40.48′E	21.7–21.8	IR-OSL	55.5 ± 5.1	157.0 ± 11.0	0.36	1.52	1.73	This paper
RLQG 1521-103	66°13.65′N, 39° 40.53′E	22.6–22.7	IR-OSL	44.4 ± 3.2	108.5 ± 4.3	0.26	2.36	1.54	Korsakova et al., 2004
RLQG 2605-069	66°13.60′N, 39°40.48′E	23.9–24.0	IR-OSL	15.4 ± 1.8	61.0 ± 0.6	1.21	4.59	2,61	This paper

[a]Sampling sites are indicated in Figs. 2 and 4–7.

Chapoma 1 section

The Chapoma 1 section (previously published as Chapoma) is located on the abrupt left slope of the Chapoma River valley, 3.5 km from its mouth (4 in Fig. 1), at an altitude up to 29–30 m asl.

In the Chapoma 1 sequence (66°6.93′N, 38°51.92′E), the lowermost weak red compact silty clay with abundant boulders, pebbles, and gravel of mainly local rocks and scarce erratic pebbles is exposed above the river shoreline, located here at ca. 10.0 m asl, and above it up to 11.05 m asl (4 in Fig. 2). The upper sharp contact, identified according to colour and changes in grain composition, dips steeply to the west. On this diamict, moisture-laden greenish-gray compact silt and silty clay (mud) with numerous shells and shell fragments, scarce pebbles, and gravel occurs at 11.5–13.6 m asl. Collected during latest study of the section from the mud, the *A. islandica* shell has been ^{230}Th/U dated to 136 ± 15/13 ka (LU-479b) (4 in Fig. 2, Table 1). Up the section, this mud is covered with silt and fine sand including abundant pebbles. Upper contact of this unit is uneven, with pockets of greenish-gray silty clay and yellowish-brown, poorly sorted, predominantly coarse sand with well-rounded pebbles; isolated weathered pebbles are represented here. Yellowish-brown, compact, poorly sorted sand with abundant boulders up to 25 cm in diameter, pebbles, and gravel occurs at 13.6–14.75 m asl. These mixed pebbly–gravelly–sandy sediments are overlain with dark grayish-brown compact silt and clayey silt with abundant rubble, differently rounded pebbles, and scarce shell fragments with a sharp and uneven contact. Above 14.75 m asl, dark grayish-brown silt gradually passes into grayish-brown and greenish-gray, weakly laminated, compact silt and sand with scarce gravel and pebble. At 14.75–17.5 m asl, thin (2–3 mm) splitting sandy laminae and scarce shell fragments are included in the silty sediments. Compact structureless clayey silt, silt, and sand with solitary rounded pebbles of local rocks and weathered far-travelled carbonate rocks occur at 17.5–18.3 m asl. At 18.3–20.0 m asl, compact silt and clayey silt with gravel and pebbles assume a special structure, breaking up into separate angular fragments; scarce fragments of shells are again visible in these deposits. The upper contact of these deposits is very uneven and sharp. At 20.0–23.5 m asl, brownish-gray, brownish-yellow, and pale-olive sands overlie the clayey silts with disconformity. Individual fragments of shells and flattened pebbles are visible in the lower part of this sand, which is IR-OSL dated to 29.1 ± 3.4 ka (RLQG 2599-069) (4 in Fig. 2, Table 1). In the sand, a deformed parting of compact dark grayish-brown silt and clayey silt occurs at 21.2–21.5 m asl. In the lower 1.5 m of this member, sands with unclear wavy bedding include pockets and angular-shaped fragments of this silt and clayey silt, as well as the broken shell fragments. A silty-clayey diapir-like fold with a disturbed fine-grained sandy core and small pockets including angular silty-clay fragments and silt is in the northern part of the outcrop. At 22.3–23.5 m asl, strongly deformed sand, silt, and clayey silt, including lenses and pockets with gravel and pebbles, as well as pockets of ripple bedding sand with individual very small shell fragments are presented. Two different IR-OSL dates were obtained from this deformed part of the Chapoma 1 section, namely, 23.0 ± 2.7 ka (RLQG 2600-069) from the sand at 22.5 m asl and 76.7 ± 8.9 ka (RLQG 2601-069) from the sand at 23.3 m asl (4 in Fig. 2, Table 1). Upward, dark olive-gray homogenized diamicton represented by compact clayey silt with boulders, pebbles, and gravel lies on the deformed sandy deposits with sharp uneven contact

https://doi.org/10.1017/qua.2024.24 Published online by Cambridge University Press

at 23.5–27.5 m asl. The top of the Chapoma 1 outcrop is covered by turf up to 29.0 m asl.

Chapoma 2 section

The Chapoma 2 section is located 0.05 km from the Chapoma River mouth at the junction of the abrupt left slope of the river valley and an eroded sea cliff up to 23.8 m asl (Zaretskaya Mount) (5 in Fig 1). This section was previously published as Faktoria (Zaretskaya et al., 2022).

The Chapoma 2 sedimentary sequence was observed in two trenches spaced 40 m apart (5S and 5N in Fig. 2). Basal sedimentologic units were studied in the trench located in the southern part of the outcrop (66°6.22′N, 38°53.18′E) facing the White Sea shore (5S in Fig. 2). At ca. 6.0 m asl, a basal shingle and boulders are covered with compact very dark gray clayey silt, which gradually changed to dark-gray clayey silt and silt up to 8.9 m asl. These deposits contain scarce shell detritus, gravel, and pebbles. In the uppermost part of this unit, 0.10- to 0.12-m-length lenses and pockets with gray wavy-laminated fine sand occur. The upper contact, detected by particle-size distribution and colour, is distinct and uneven, with fragments of clayey silt intercalated into overlying sediments. Above this erosional contact marked with well-rounded pebbles, loose, indistinctly horizontally laminated, reddish-brown, poorly sorted, predominantly coarse sand with red arkosic sandstone cobbles, well-rounded gravel, and very small shell fragments were observed. In the southern trench, the apparent thickness of these sediments is ca. 1 m; upward, talus covers the coastal slope. The sand sample taken from basal part was IR-OSL dated to 95.3 ± 8.1 ka (RLQG 2661-070) (Zaretskaya et al., 2022; 5S in Fig. 2, Table 1).

Other sedimentary units of the Chapoma 2 sequence were studied in the northern part of the outcrop (66°6.27′N, 38°53.15′E) facing the river valley (5N in Fig. 2). Here, dark grayish-brown fine sand and silt with shell fragments and small pebbles is exposed in the basal part of the sequence; festooned flame-like structures, seams, and pockets formed by gray fine sand or reddish-gray medium sand occur here. A sand sample at 7.5 m asl was IR-OSL dated to 72.4 ± 5.6 ka (RLQG 2604-069) (Zaretskaya et al., 2022; 5N in Fig. 2, Table 1). These lowermost deformed sandy and silty deposits were observed here at 6.0–8.5 m asl in the form of a lens, which seems to be leaning against the clayey silt, silt, and sand exposed in the Chapoma 2 south section (5S in Fig. 2). Along the stretch of outcrop, these deformed sediments in section 5N replace the clayey silt, silt, and sand visible in section 5S. Upper contact of this member is not clearly visible due to thick talus; its location was roughly identified according to implicit data. Upward, the thick sandy unit, identified at 8.5–14.15 m asl, is composed of gray and reddish-gray fine and medium sand with shell fragments and displays horizontal and wavy lamination throughout the entire thickness. In its upper part, lenses and interbeds of gravel and coarse sand with shell fragments, sparse flattened arkosic sandstone cobbles, and pockets of horizontal, weakly laminated, fine-grained sand are visible at 14.0–14.15 m asl. Above them at 14.15–16.8, predominantly wavy or oblique laminated sand was IR-OSL dated to 36.2 ± 2.8 ka (RLQG 2603-069) and 32.5 ± 3.8 ka (RLQG 2602-069) (Zaretskaya et al., 2022; 5N in Fig.2, Table 1). At 16.8–17.5 m asl, compact dusky red with thin interbeds of dark-gray fine sand occurs; the lower contact is clear, uneven, and identifiable by colour and grain-size composition. At 17.5–23.8 m asl, a compact dark reddish-gray diamicton, represented by silt with gravel and pebbles and having a platy structure, turning upwards into massive clayey silt, is observed; an interbed of pale-brown, poorly sorted, predominantly fine sand with 0.2-m-thick included well-rounded gravel and pebbles occurs in the middle part of this unit. The diamicton overlaps the underlying sands, with a gradual transition marked with a pocket of fine sand.

Bolshaya Kumzhevaya section

The Bolshaya Kumzhevaya section (66°13.60′N, 39°40.48′E) is located on the steep left bank of the Bolshaya Kumzhevaya River valley, 3.1 km from the mouth of the river at an altitude of 16–27 m asl (6 in Fig. 1). The natural outcrop exposes a wide terrace composed of marine and glacial deposits and is located 200 m from its bench, which has a steepness of about 45° and a relative height of about 10 m.

In the basal part of the Bolshaya Kumzhevaya sequence (6 in Fig. 2), water-bearing grayish-green fine sand and silt with gravel and rounded pebbles occur at 16.0–18.0 m asl; the complanate large pebbles and scarce boulders are oriented subhorizontally. Upper contact is sharp, identified by colour and grain composition. At 18.0–18.5 m asl, subbasal grayish-brown 0.1-m-thick silt with gravel and pebbles is overlain by water-bearing black and dark-gray, 0.1-m-thick, poorly sorted, predominantly medium sand with cobbles located under pockets of coarse sand and gravel, which gradually change upward into dark grayish-brown and brown, 0.3-m-thick medium sand with pockets of coarse sand, scarce gravel, and cobbles. The sand at 18.25 m asl was IR-OSL dated to 95.9 ± 6.3 ka (RLQG 2660-070) (6 in Fig. 2, Table 1). The thick sandy unit, identified at 18.5–23.5 m asl, is composed of three beds. The lower one is represented by light yellowish-brown 0.7-m-thick thin sand with horizontally weak lamination and differently directed oblique lamination underlying light brownish-gray, weakly laminated, thin sand and silt of 0.4 m thick; a sand sample at 19.6 m asl was IR-OSL dated to 57.6 ± 6.7 ka (RLQG 2607-069) (6 in Fig. 2, Table 1). Upward, this sand changes to 0.7-m-thick massive grayish-brown thin sand with scarce gravel and small pebbles, which is overlaid by 1.7-m-thick, horizontal, weakly laminated, thin sand IR-OSL dated to 55.5 ± 5.1 ka (RLQG 2606-069) at 21.55 m asl (6 in Fig. 2, Table 1). The uppermost bed is composed of horizontal or wavy weakly laminated thin sand with thin interbeds and pockets of light brownish-gray silt and medium sand. The upper erosional contact of this sandy layer is clear, uneven, and identifiable by colour and grain-size composition. Upward, reddish-gray diamicton represented by compact silty clay splitting into indistinct horizontal thin plates and clayey silt with boulders, pebbles, and gravel lies on the sandy member with sharp uneven contact at 23.5–27.0 m asl. A 0.25-m-thick parting of pinkish-gray, wavy laminated, fine sand and silt, IR-OSL dated to 15.4 ± 1.8 ka (RLQG 2605-069) (6 in Fig. 2, Table 1), with erosional sharp contacts, occurs at 23.9 m asl.

Discussion

The reliability of the dating results

To validate the reliability of the IR-OSL dates presented in this paper (Table 1), we provide a series of comparative results obtained earlier using two methods: IR-OSL and ESR (Fig. 3, Table 2). These results mainly stem from parallel dating using ESR and IR-OSL techniques on shells and feldspar grains,

https://doi.org/10.1017/qua.2024.24 Published online by Cambridge University Press

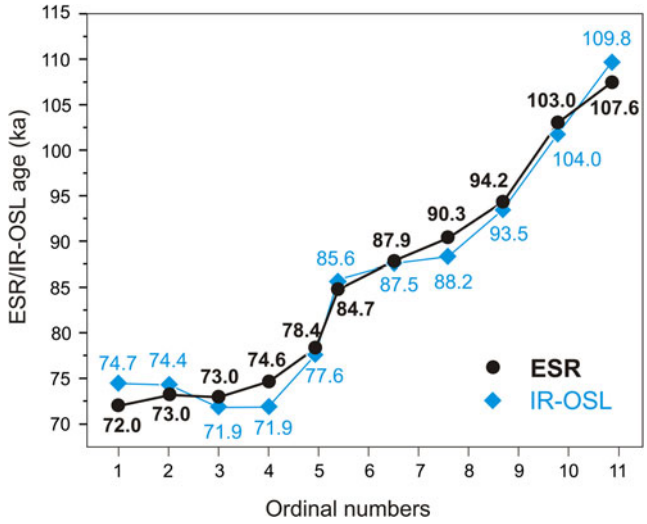

Figure 3. Comparison of parallel dating results obtained by two main independent dating methods used in the present study: electron spin resonance (ESR) and infrared optically stimulated luminescence (IR-OSL). The figure indicates the ages (in ka).

respectively, extracted from the same sediment sample. Our comparative results showcase the potential of both combined and independent palaeodosimetric dating methods applied to two different minerals— biogenic carbonate and feldspar—to chronologically organize middle to late Pleistocene palaeoenvironmental events.

The results obtained are particularly significant due to frequent references in the literature to challenges such as incomplete bleaching of sediment grains. Such incomplete bleaching may result from factors like transport in turbid waters with high suspended particle concentrations or reworking of initial subaqueous sediments. These factors, or similar ones, would be expected for marine sediments, potentially leading to age overestimations. Additionally, it is assumed that alkali feldspars exhibit specific athermal (anomalous) fading of their luminescence, which could hinder the reliable luminescence dating of Quaternary deposits based on feldspar extractions, potentially causing unpredictable age underestimations. For instance, Wallinga et al. (2001) reported a nearly 50% underestimation of feldspar IR-OSL ages compared with quartz OSL ages measured on the same samples, presumably due to anomalous fading.

The reliability of the palaeodosimetric dating techniques employed in this study is also demonstrated through the series of comparative results obtained using a series of independent numerical dating methods, such as K-feldspar-based IR-OSL, mollusc shell–based ESR, quartz-based optically stimulated afterglow, U-Th, and ^{14}C, applied to the same sedimentary samples (Molodkov, 2020), as well as relative dating methods (Molodkov, 2012). A notable consistency observed in dating results from feldspar and quartz grains, as well as mollusc shells taken from the same sedimentary context, indicates no noticeable athermal fading of feldspar dosimetric traps over geologic timescales, as detailed in previous studies (Vasilchenko et al., 2005; Molodkov et al., 2007; Jaek et al., 2008, 2010), nor does it indicate incomplete bleaching of sediment grains, even under complex conditions expected in marine environments.

The results obtained using the $^{230}Th/U$ age radioisotope method on subfossil thick-walled, well-preserved mollusc shells are somewhat questionable due to the potential open-system behaviour of subfossil shells with respect to uranium (see Kaufman et al., 1996). In the postsedimentation period, the shells can be subject to both secondary uranium enrichment, as a result of their contact with marine or ground water, and leaching of uranium and thorium compounds. In addition, it is possible for mineral suspension to penetrate into shells, leading to thorium contamination, which is detected by the presence of the ^{232}Th isotope (Choukri et al., 2007; Rowe et al., 2015). Thus, the reliability of $^{230}Th/U$ age, depending on the local conditions of shell fossilization, is not an accurate radioisotope chronometer and can rather be used to approximate the age of the enclosing sediments (Labonne and Hillaire-Marcel, 2000; Choukri et al., 2007).

Interpretation of sedimentary successions and depositional environments

In accordance with the regional subdivisions of the late Pleistocene derived from previous reconstructions (Molodkov

Table 2. Results of parallel dating of the same marine sediment sample using mollusc-based electron spin resonance (ESR) and feldspar-based infrared optically stimulated luminescence (IR-OSL) methods.

Sample no.[a]	Lab no. (ESR/IR-OSL)	ESR age (ka)	IR-OSL age (ka)	References
1	RLQG 319-042/1477-103	72.0 ± 4.8	74.7 ± 8.3	Zarkhidze et al., 2010
2	RLQG 400-039A-B/1862-039	73.0 ± 4.0	74.4 ± 6.8	Molodkov and Bolikhovskaya, 2010
3	RLQG 396-039/1861-039	73.0 ± 7.5	71.9 ± 8.2	Molodkov and Bolikhovskaya, 2010
4	RLQG 449-061A-D/2043-081	74.6 ± 3.1	71.9 ± 5.6	Gusev and Molodkov, 2012
5	RLQG 489-094/2254-054	78.4 ± 6.4	77.6 ± 6.0	Gusev et al., 2016
6	RLQG 490-094/2270-094	84.7 ± 7.0	85.6 ± 6.7	Gusev et al., 2016
7	RLQG 455-052/2077-052	87.9 ± 4.2	87.5 ± 6.8	Gusev et al., 2016
8	RLQG 317-042/1608-124	90.3 ± 10.9	88.2 ± 5.4	Zarkhidze et al., 2010
9	RLQG 491-104/2255-104	94.2 ± 7.8	93.5 ± 7.3	Gusev et al., 2016
10	RLQG 310-042A-D/1405-031	103.0 ± 4.2	104.0 ± 8.3	Molodkov and Yevzerov, 2004
11	RLQG 318-042/1478-103	107.6 ± 12.4	109.8 ± 6.9	Zarkhidze et al., 2010

[a]Sampling locations: samples 2, 3, and 10: Kola Peninsula; samples 1, 8, and 11: the easternmost coastal area of the Barents Sea; samples 4–7 and 9: the Kara Sea coastal area.

https://doi.org/10.1017/qua.2024.24 Published online by Cambridge University Press

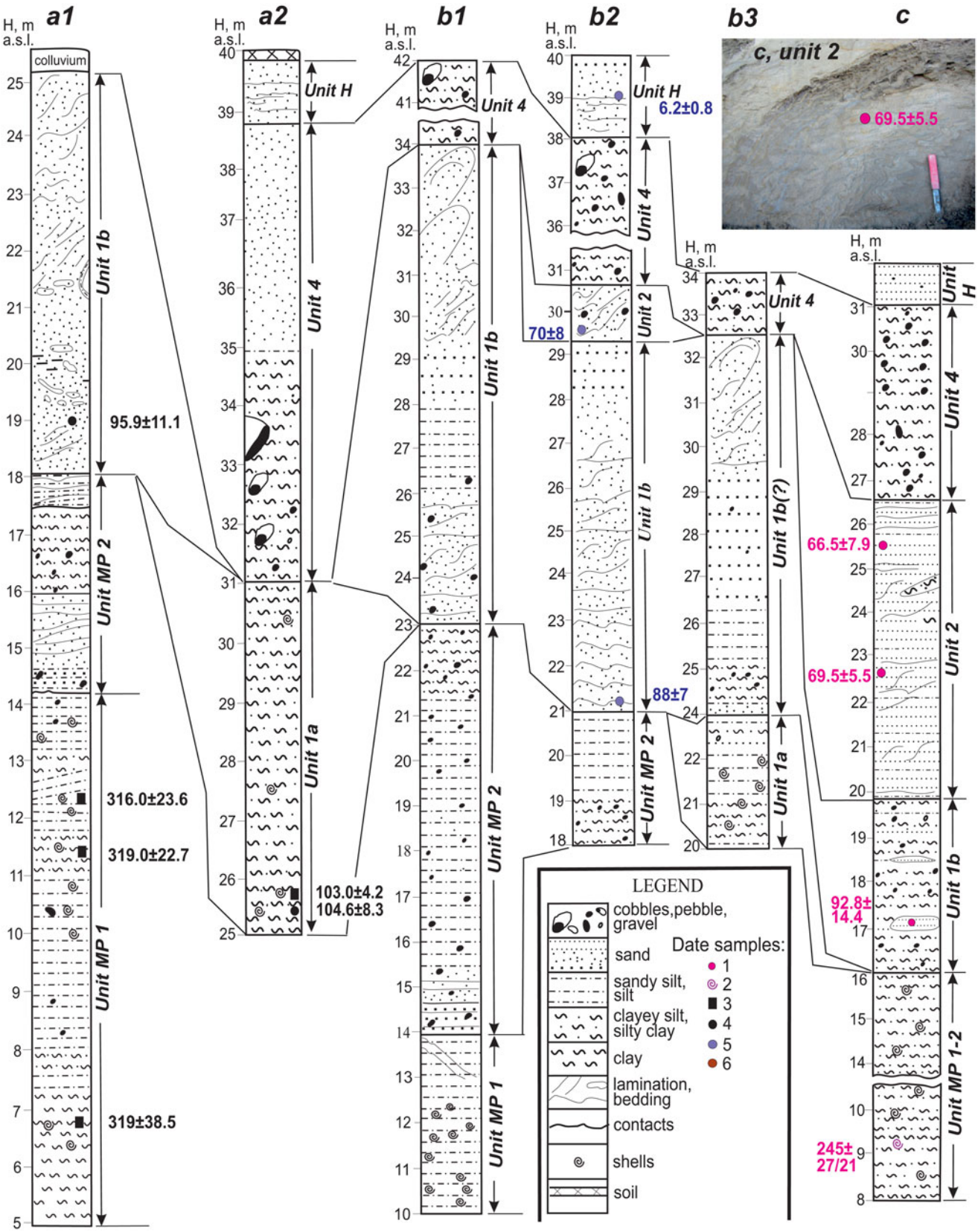

Figure 4. Late Pleistocene sedimentologic successions from the Varzuga sequence: sections 1a and 1b derived from Korsakova et al. (2016); sections b1, b2, and b3 derived from Lunkka et al. (2018); section c presented in this paper. Date samples and dating results: 1, infrared optically stimulated luminescence (IR-OSL) (this paper); 2, ^{230}Th/U (this paper); 3, electron spin resonance (ESR) (Korsakova et al., 2004, 2019; Molodkov and Yevzerov, 2004); 4, IR-OSL (Molodkov and Yevzerov, 2004; Korsakova et al., 2019); 5, OSL (Lunkka et al., 2018); 6, ^{230}Th/U (Arslanov et al., 1981). The main subdivisions are designated as units correlating with the Marine Isotope Stages (MIS) according to presented data: MP (MIS 9), MP 2 (MIS 8–6), U1a and U1b (MIS 5 with corresponding Ponoy and Strelna beds, respectively), U2 (MIS 4), U3 (MIS 3), U4 (MIS 2), and H (MIS 1).

https://doi.org/10.1017/qua.2024.24 Published online by Cambridge University Press

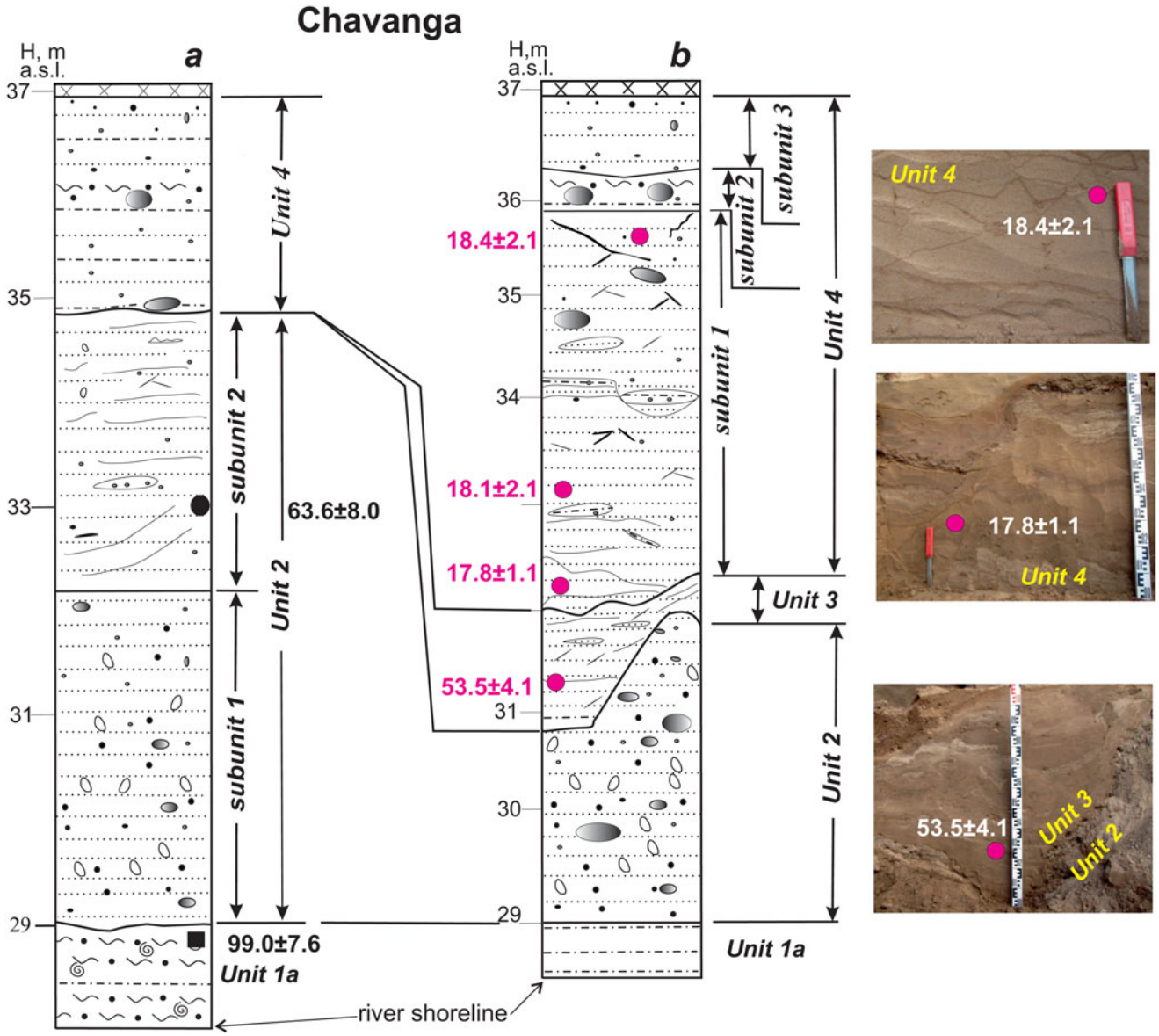

Figure 5. Late Pleistocene sedimentologic successions from the Chavanga sequence: section a derived from Korsakova et al. (2004); section b presented in this paper. See Fig. 4 legend for symbols.

and Bolikhovskaya, 2002; Korsakova et al., 2004, 2016, 2019; Korsakova, 2019, 2021; Zaretskaya et al., 2019, 2022), the stratigraphic sequence is subdivided into four informal lithostratigraphic formations (units and subunits). These units are U1 (MIS 5 warming) and corresponding marine (m) Ponoy (U1a) and Strelna (U1b) beds; then U2 (severe cooling correlated to MIS 4) and U3 (a time interval with complex and variable environment correlated to MIS 3) (see, e.g., Kind, 1974; Bolikhovskaya and Molodkov, 2007), represented mainly by glaciomarine (gm) and marine (m) formations, as well as glacial (g) and glaciofluvial (f) deposits; and U4 (MIS 2 cooling) represented by deposits interpreted as glacial (g), glaciofluvial (f), glaciolacustrine (l), and glaciomarine (gm). In the studied sequences, Unit H includes mainly the Holocene marine, aeolian, and other terrestrial surficial deposits; middle Pleistocene deposits known in the Kola Peninsula correlate with Units MP 1 (MIS 9) and MP 2 (nonsegmented glacial–interglacial beds, MIS 8–6) (Korsakova et al., 2019).

Varzuga sequence

In the Kola region, sedimentary sequences exposed in the Varzuga outcrop (Figs. 2 and 4) represent the most complete and longest record of late Pleistocene history over the MIS 5–4 stages. Earliest late Pleistocene dark brownish-gray mud with dominating clayey silt includes shells and shells fragment (Unit 1a), and overlying laminated, cross-bedded, sandy and silty sediments (Unit 1b) were described in the Varzuga outcrop. Previous investigations (Korsakova et al., 2004, 2019; Molodkov and Yevzerov, 2004) showed that along the stretch of the outcrop downstream of the Varzuga River, the Unit 1b sandy and silty sediments are partly replaced by clayey silt containing mollusc shells (Unit 1a) at 25–31 m asl (Fig. 4, sections a1 and a2). The weighted mean of several ESR age determinations on different shells from the Unit 1a clayey silt was estimated at 103.0 ± 4.2 ka (RLQG 309-12-042), which agrees with the age of 104.0 ± 8.3 ka (RLQG 1405-031) obtained by IR-OSL on potassium feldspar extracted from the enclosing deposits (Molodkov and Yevzerov,

https://doi.org/10.1017/qua.2024.24 Published online by Cambridge University Press

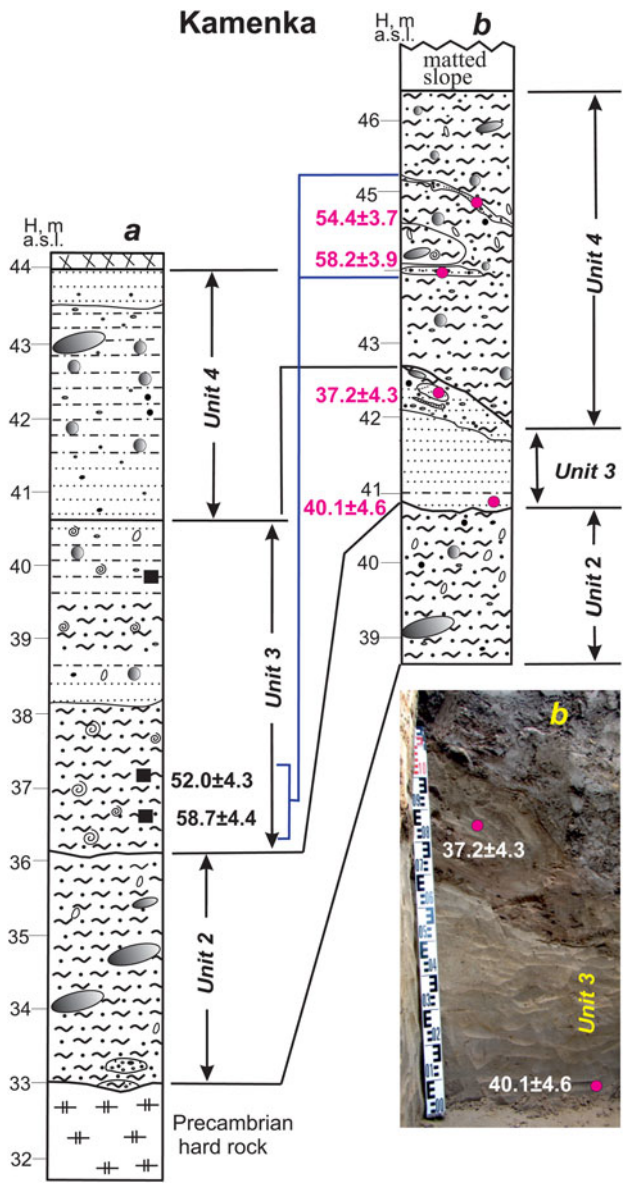

Figure 6. Late Pleistocene sedimentologic successions from the Kamenka sequence: section a derived from Korsakova et al. (2004); section b presented in this paper. See Fig. 4 legend for symbols.

2004). The Unit 1a sediments are also suggested in Varzuga section b3 (Fig. 4) in accordance with its stratigraphic position in the sequence presented by Lunkka et al. (2018). The lowermost part of the sandy Unit 1b was later dated by IR-OSL at 95.9 ± 11.1 ka (Korsakova et al., 2019; Fig. 4, section a1) and by OSL at 88 ± 7 ka (Lunkka et. al., 2018; Fig. 4, section b2).

The juxtaposing of lithologic and chronological data from several sediment successions studied by many researchers (Fig. 4, Table 1) provide evidence that the late Pleistocene depositional sequences in the Varzuga sections show four formations (Units 1a, 1b, 2, and 4 in Fig. 4); three sharp contacts suggested erosional events throughout the depositional history. The Unit 1a sediment succession with clayey and silty deposits including warm-water molluscan fauna, as well as foraminifera and diatoms (Gudina and Yevzerov, 1973), that is, Ponoy beds in the regional stratigraphy (Korsakova, 2019), is locally present in the Varzuga sections and has been identified in a few points at ca. 25–31 and 20–24 m asl (Fig. 4, sections a2 and b3, respectively), indicating its lens-shaped bedding. Results of multimethod chronological investigations (Molodkov and Yevzerov, 2004) show that Unit 1a was formed here at 104–103 ka (Fig. 4, section a2, Table 1), which corresponds to further development of the interglacial warm-water Boreal marine transgression in the White Sea depression. Unit 1b is correlated to one or more interglacial marine events in the Kola Peninsula known in the regional stratigraphic scheme as the Belomorian transgression (Lavrova, 1960; Korsakova et al., 2016, 2019), which is suggested to be the final phase of the Boreal marine transgression (about 110–70 ka). In the Varzuga sequence, sandy and silty sediments of Unit 1b dated to 95.9, 92.8, and 88.0 ka (Fig. 4, sections a1 and b2, Table 1) sharply overlie silty sediments of Unit 1a (Ponoy beds) in section b3; their composition suggests the ca. 1.0-m-thick transgression succession at 24–25 m asl and a thicker regression at 25–32.5 m asl. In sections a1, b1, b2, and c (Fig. 4), the Unit 1b deposits sharply overlie the middle Pleistocene sediments with erosion. Although there is the opinion (Lunkka et. al., 2018) that the basal part of this unit (i.e., lower 1.0-m-thick transgression succession of Unit 1a in section b3 in Fig. 4) represents subglacially deformed sediments or mass movement diamicton conformably overlain by laminated silt (i.e., several meters thick regression succession in section b3 in Fig. 4) accumulated in a basin with glaciolacustrine conditions, we suggest their marine origin because of lithology and lithostratigraphic position and correlation to other sites on the Tersky Coast. The MIS 4 deposits were identified because of the new geochronological data from the uppermost part of Unit 2 in section c, which was dated to 69.5 ± 5.5 (RLQG 2613-079) and 66.5 ± 7.9 ka (RLQG 2614-079), as well as from basal part of Unit 2 in section b2 dated to 70 ka (Lunkka et al, 2018; Fig. 4, Table 1). Unit 2, which is composed of sandy deposits, should have consistently accumulated during a cold environment, which, according to geochronological data, is comparable to the cold MIS 4. The origin of these sandy deposits can only be assumed with a high degree of uncertainty. It is most likely that the Unit 2 sediment accumulated in unstable coastal and shallow-water environments, possibly in a marine setting, for example, during the Mezen transgression, which developed in this region during MIS 4 (Zaretskaya et al., 2022). The late Valdaian (late Weichselian, MIS 2) clayey silt of Unit 4 overlaps sandy Unit 2 with sharp contact and erosion (Fig. 4), which demonstrates a hiatus in the middle–late Valdaian (middle–late Weichselian) interglacial–glacial sediment succession. In the Varzuga sections, the observed sedimentary sequences show listric folds, thrust planes, and other folded structures in the sandy deposits underlying the Unit 4 sediments; these structures are associated with the glaciotectonic impact of the SIS (Lunkka et. al., 2018; Korsakova et al., 2019). The uppermost Unit H sediments were attributed to the end of the late glacial and Holocene, suggesting their lacustrine and aeolian origin (Lunkka et. al., 2018). In the lower Varzuga River area, the vast aeolian landscapes are presented now in the coastal zone.

Chavanga sequence

Units 1a–2–3–4 sedimentologic succession was identified in the Chavanga outcrop (Figs. 2 and 5). Previously investigated (Gudina and Yevzerov, 1973; Korsakova et al., 2004), section a (Fig. 5) demonstrates the Unit 1a deposits with fragments and valves of subfossil shells of arctic, arctic–boreal, and boreal mollusc species ESR dated to 99.0 ± 7.6 ka (Fig. 5, Table 1). Unit 1a

https://doi.org/10.1017/qua.2024.24 Published online by Cambridge University Press

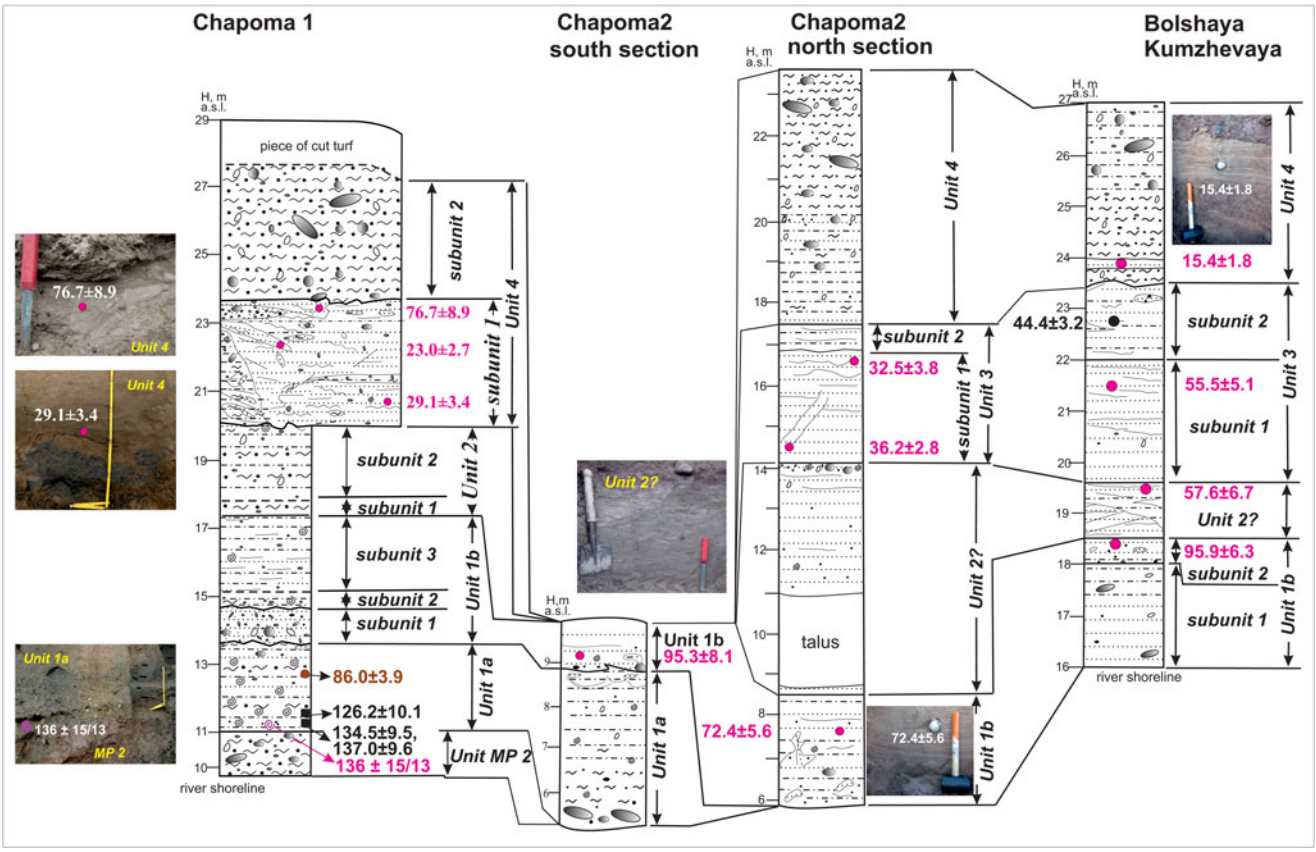

Figure 7. Late Pleistocene sedimentary successions from the Chapoma 1, Chapoma 2, and Bolshaya Kumzhevaya sequences. See Fig. 4 legend for symbols.

was attributed to Ponoy beds accumulated in the end of initial phase of the Ponoy transgression, which corresponds to the first phase of the Boreal transgression. These sediments are sharply overlaid with erosion by the Unit 2 pebbles and gravels in a sandy and silty matrix (subunit 1, section a in Fig. 5) covered by laminated sands with rounded pebbles (subunit 2, section a in Fig. 5). Here, subunit 2 of Unit 2 (section a in Fig. 5) is similar to Unit 2 in the Varzuga sequence, specifically section c (Fig. 4), because of its lithology and chronology, suggesting similar settings during their accumulation in MIS 4 under marine environments. The 53.5 ± 4.1 ka date (section b in Fig. 5, Table 1) could indicate a longer accumulation stage in the marine environment, embracing part of MIS 4 and the onset of MIS 3. Subunit 2 of Unit 2, dated to 63.65 ± 8.0 ka (section a in Fig. 5, Table 1), and laminated sand of Unit 3 (section b in Fig. 5) have a marine origin and accumulated in unstable coastal and shallow-water environments. Based on lithologic composition, it can be interpreted that subunit 1 of Unit 2 could have accumulated in MIS 4 in a glaciofluvial setting. The late Valdaian (late Weichselian, MIS 2) Unit 4 is subdivided into three subunits (section b in Fig. 5). Dated to 18.1–17.8 ka, sand of subunits 1 with folded structures and thrust planes can be identified as deformed till that was deposited during the last glacial/ice sheet advance. Subunits 2 and 3 of Unit 4 can be interpreted as supraglacial allochthonous sediments.

Kamenka sequence

A reduced Units 2–3–4 sedimentary sequence is represented in the Kamenka outcrop (Figs. 2 and 6). This sedimentary succession was previously investigated (Gudina and Yevzerov, 1973; Korsakova et al., 2004; Astafiev et al., 2012). The silty clay and sand of marine units sandwiched here with sharp contacts between the diamicton indicated by pebbles and gravel in a clayey, silty, or sandy matrix (section a in Fig. 6) were recognized. As in other sequences on the Tersky Coast, Unit 2 is correlated to MIS 4. Here, Unit 2 consists of a glacial diamicton, which is superposed by marine sediments overlapping it with erosion. The glacial origin of the Unit 2 gravelly silty clay was recognized according to its lithologic composition and lithostratigraphic position below the silty clay, silt, and sand with mollusc shells and marine diatoms (Gudina and Yevzerov, 1973). Fragments of subfossil shells of arctic–boreal and arctic mollusc species, that is, *Mya* sp., *Chlamys islandica*, *Astarte crenata*, and *Astarte crebricostata*, as well as marine diatoms *Isthmia* sp., *Isthmia nervosa*, *Rhabdonema* sp., and *Paralia sulcata* (Grave et al., 1969; Korsakova, 2021), were found in silty clay, silt, and sand corresponding to Unit 3 (section a in Fig. 6). The Unit 2 diamicton, demonstrating structures in the form of indistinct horizontal thin partings into thin microplate and underlying marine sediment with uneven sharp contact, appears to be a basal till and can be correlated with the MIS 4 glacial event on the Kola Peninsula. Accumulation of the Unit 3 marine sediments, dated to 37.2 ± 4.4 ka (RLQG 2612-079) and 40.1 ± 4.6 ka (RLQG 2611-07) (section b in Fig. 6, Table 1), suggests a cold-water basin with a changing coastline during the time interval 58–37 ka (Fig. 6, Table 1) correlated to MIS 3. No thermophilic diatom species have been found here; the mollusc shells from the lower part of this unit were ESR dated to 58.7 ± 4.4 (RLQG 344-073)

https://doi.org/10.1017/qua.2024.24 Published online by Cambridge University Press

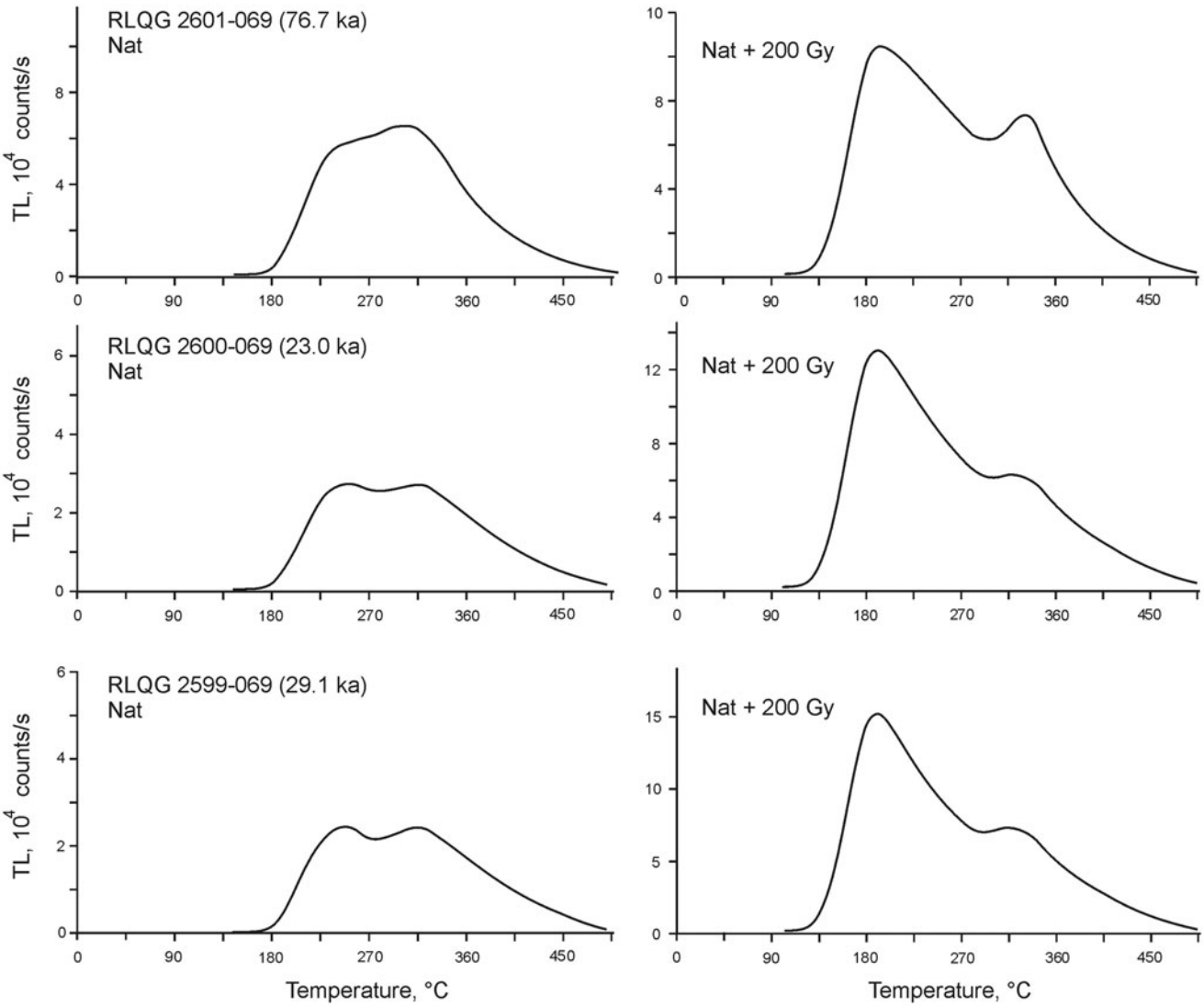

Figure 8. Thermoluminescence (TL) glow curve shapes for natural (left) and irradiated to 200 Gy (right) potassium feldspar grains extracted from sedimentary samples RLQG 2599-069 (29.1 ± 3.4 ka), RLQG 2600-069 (23.0 ± 2.7 ka), and RLQG 2601-069 (76.1 ± 5.9 ka) taken from the Chapoma 1 section at 20.5, 22.3, and 23.4 m asl, respectively.The TL glow curve shapes of the natural and irradiated feldspar grains are practically indistinguishable for the two lower samples dated back to 29.1 ka and 23.0 ka, but the two lower samples diverge significantly from the upper sample dated back to 76.1 ka. This suggests a similarity in the chemical and physical environments during the crystallization of the feldspars in the two lower samples throughout their geologic history and a contrast with the conditions for the upper sample. Consequently, it is inferred that the sedimentary material in the upper layer originated from a different source area than the sediments in the lower layers.

and 52.0 ± 4.3 (RLQG 416-119) ka (Korsakova et al., 2004; Astafiev et al., 2012; Fig. 6, Table 1). Spores from these sediments show that a forest–tundra with sparse growth of *Betula–Pinus* trees covered the adjacent land (Grave et al., 1969). The uppermost part of the Kamenka sequence, that is, Unit 4, appears to be waterfront glacial sediments represented by glaciomarine deformed till with pockets of allochthonous inclusions originated most probably from underlying marine deposits, IR-OSL dated to 58.2 ± 3.9 ka (RLQG 2662-070) and 54.4 ± 3.7 ka (RLQG 2663-070) (Fig. 6, Table 1). The top position of Unit 4 in the sequence indicates its late Valdaian (late Weichselian, MIS 2) age.

Chapoma 1 sequence

In the Chapoma 1 (Figs. 2 and 7), Units 1a–1b–2–4 sediment succession was suggested. In the twentieth century, this sequence was studied by Lavrova (1960), Malyasova (1960), Cheremisinova (1962), Grave et al. (1969), Gudina and Yevzerov (1973), and Arslanov et al. (1981). Corresponding litho-, bio-, and chronostratigraphic data were summarized in Korsakova (2019, 2021). The data previously obtained demonstrate that compact silty clay with gravel, pebbles, and boulders and scarce marine foraminifera (Grave et al., 1969) comprises the lowermost part of the sequence (Unit MP 2 in Fig. 7). Upwards with a sharp contact, silt and silty clay (Chapoma 1 section, Unit 1a in Fig. 7) with abundant subfossil mollusc shells of *A. islandica* and *Astarte elliptica* ESR dated at 126.2 ± 10.1 ka (RLQG 267-129) (Molodkov and Bolikhovskaya, 2002), 134.5 ± 9.5 ka (RLQG 395-039A) and 137.0 ± 9.6 ka (RLQG 395-039B) (Molodkov, 2012) were identified. The lower part of this unit was ^{230}Th/U dated at 136 ± 15.13 ka and the upper part at 86.0 ± 3.9 ka (Chapoma 1 section in Fig. 7, Table 1). The latter is a very preliminary date, because this was the first attempt to date shells by ^{230}Th/U method in the Kola Peninsula.

https://doi.org/10.1017/qua.2024.24 Published online by Cambridge University Press

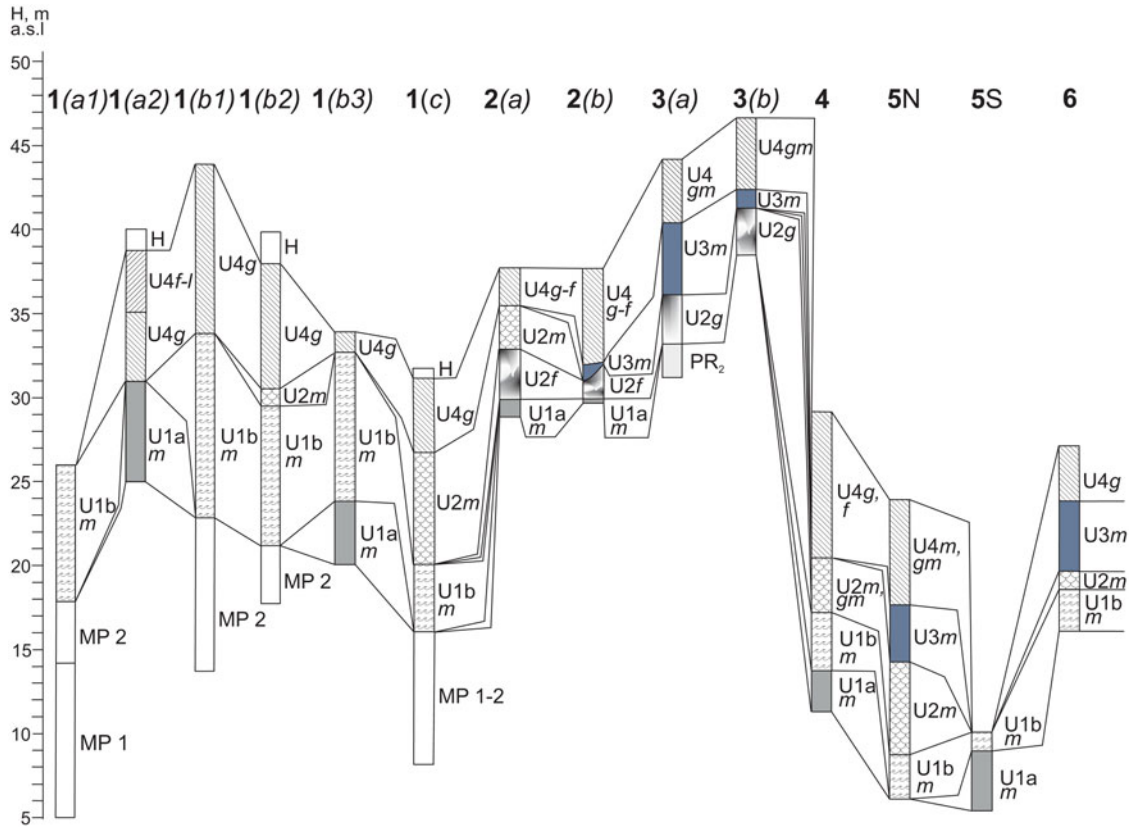

Figure 9. Late Pleistocene lithostratigraphic units and correlations of the studied sequences. The numbers 1–6 indicate the sections under consideration; their locations are shown in Fig. 1. Lithostratigraphic units (U) correspond to those in Figs. 4–7; the genesis of sediments is shown by letters: g, glacial; f, glaciofluvial; l, glaciolacustrine; gm, glaciomarine.

According to available data, the Unit 1a compact silt and silty clay with numerous shells and shell fragments, scarce pebbles, and gravel started to accumulate at ca. 138–128 ka and can be attributed to the initial phase of the interglacial Boreal transgression. The abundant fauna and diatoms suggest hydrobiological conditions in that marine basin to be more favourable than those of the present-day White Sea (Cheremisinova, 1962; Grave et al., 1969; Gudina and Yevzerov, 1973; Korsakova, 2021), likely due to the influence of the warm North Atlantic Current (Zatsepin and Filatova, 1961; Funder et al., 2002; Grøsfjeld et al., 2006). The Unit 1b sediments with shells superpose the Unit 1a with a sharp erosional contact, suggesting some gap in the marine sedimentation. Successively overlaid, pebbly and gravelly sand (subunit 1 of Unit 1b in the Chapoma 1 sequence in Fig. 7), a thin layer of silt (subunit 2 of Unit 1b in the Chapoma 1 sequence in Fig. 7), and weakly laminated silty-sandy deposits (subunit 3 of Unit 1b in the Chapoma 1 sequence in Fig. 7) appear to be the attributable to the latter half of the Boreal transgression (Molodkov and Yevzerov, 2004), which can be correlated with MIS 5c–a. In the Chapoma 1 sequence, Unit 2 clayey silt and silt with scarce shell fragments can be interpreted as the sedimentary succession associated with the shallowing marine basin that existed during the final phase of MIS 5a and onset of MIS 4. Subdivided into subunits, Unit 4 is similar to Unit 4 in the Chavanga sequence (section b in Fig. 5). In the Chapoma 1 sequence, subunit 1 of Unit 4 was dated by three samples at 29.1 ± 3.4 ka (RLQG 2599-069), 23.0 ± 2.7 ka (RLQG 2600-069), and 76.7 ± 8.9 ka (RLQG 2601-069) (Fig. 7, Table 1). The last, in addition to reliable IR-OSL dating, is confirmed by the results of TL analysis performed on all three samples of subunit 1 of Unit 4. Figure 8 shows that the TL curves of feldspars from RLQG 2599-069 (29.1 ka) and RLQG 2600-069 (23.0 ka) exhibit a striking similarity, whereas the curve for RLQG 2601-069 (76.7 ka) displays noticeable differences. This observation suggests that the source areas for samples dated at 29.1 ka and 23.0 ka share a relatively consistent origin, unlike the third sample. It appears that the material corresponding to this sample, dated at 76.6 ka (MIS 5a), originated from a distinct source, most likely of marine origin, and was redeposited through various physical processes. In this case, it is probable that the redeposition occurred due to the action of glacier ice. Subunit 2 of Unit 4 (Chapoma 1 section in Fig. 7) is suggested to be a basal till. In previous studies, glaciofluvial coarse-grained sediments were identified in the uppermost part of Unit 4 in the Chapoma 1 sequence (Gudina and Yevzerov, 1973; Korsakova, 2021).

Chapoma 2 sequence

In the Chapoma 2 outcrop (Figs. 2 and 7), lithologic and chronological data suggest the late Pleistocene Units 1a–1b–2–3–4 sediment succession. Clayey silt and silt of Unit 1a in the Chapoma 2 sequence are attributable to the initial phase of the Boreal transgression, as their lowermost lithostratigraphic position under marine sandy member (Unit 1b) was dated with the IR-OSL method to 95.3 ± 8.1 ka (RLQG 2661-070) in the Chapoma 2 south section and 72.4 ± 5.6 ka (RLQG 2604-069) in the Chapoma 2 north section (5N in Fig. 7), with the south and

https://doi.org/10.1017/qua.2024.24 Published online by Cambridge University Press

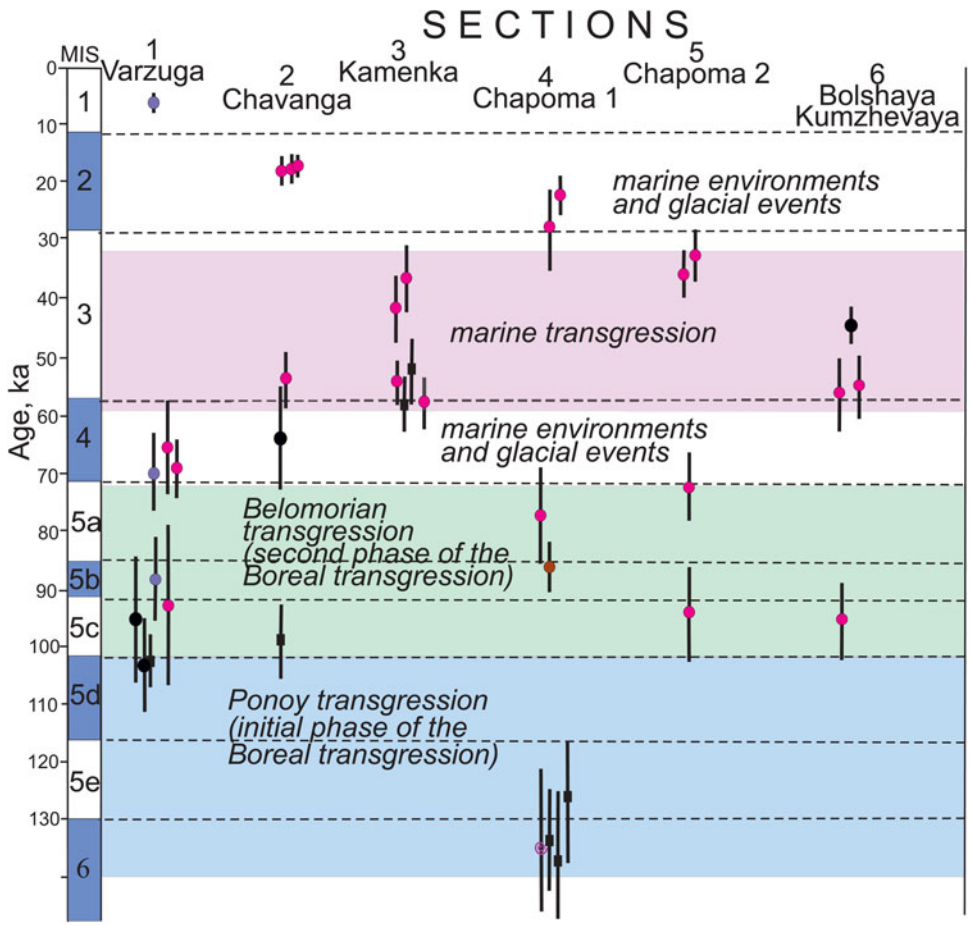

Figure 10. Late Pleistocene marine and glacial events in the Kola Peninsula coastal area. The numerical age is indicated by symbols as per the legend in Fig. 4. See Table 1 for details on dates.

north sections being located about 40 m apart. In the north section at the Chapoma 2 site, a late phase of the Boreal transgression (Belomorian transgression) is marked by silt and sand IR-OSL dated to 72.4 ± 5.6 ka (Unit 1b in the Chapoma 2 north section, Fig. 7). Here, Unit 2 sand is correlated to MIS 4 according to its lithostratigraphic position in the sequence; sedimentologic features of this sand, which is locally laminated, included flattened pebbles and shell fragments and interbedded with gravel, demonstrate its accumulation in the shallow-water marine environments of the Mezen transgression (Zaretskaya et al., 2022). The overlying wavy or oblique laminated sand of subunit 1 of Unit 3, IR-OSL dated to 36.2 ± 2.8 ka (RLQG 2603-069) and 32.5 ± 3.8 ka (RLQG 2602-069), and laminated silt of subunit 2 of Unit 3 suggest it was deposited during MIS 3 in a marine basin. The uppermost Unit 4 deposits are interpreted to be glaciomarine sediments accumulated at the glacier–sea contact during the late Valdaian (late Weichselian, MIS 2) glaciation.

Bolshaya Kumzhevaya sequence

In the Bolshaya Kumzhevaya outcrop, the Units 1b–2(?)–3–4 succession was identified based on the lithology and IR-OSL dating data (Fig. 7). This sedimentologic succession was investigated for the first time in 2003 (Korsakova et al., 2004); some differences were found only in the upper part of the excavated sequence in 2018.

The lowermost part of the Bolshaya Kumzhevaya sequence (Unit 1b in Fig. 7) consists of silty and sandy sediment that can be correlated with the second phase of the marine Boreal transgression. Judging by an IR-OSL date of 95.9 ± 6.3 ka (RLQG 2660-070) (Fig. 7, Table 1), only a minor sedimentary component of this marine event has been preserved in the section. Forming three lithologic units at 18.5–23.5 m asl and IR-OSL dated to 57.6, 55.5, and 44.4 ka (Fig. 7, Table 1), the sandy deposits accumulated in the shallow-water marine basin. The Unit 2(?) sediments suggest accumulation in an unstable littoral environment at the end of MIS 4 or at the onset of MIS 3. The Unit 3 deposits also accumulated in marine environments in early MIS 3; IR-OSL data demonstrate their MIS 3 age. No glacial or glacioaqueous sediments are obviously present in the Units 1a–3 succession here. Glacial clayey silt with sandy parting dated to 15.4 ka comprises Unit 4 and correlates with MIS 2.

Wider implications: the late Pleistocene palaeoenvironment on the Tersky Coast

The multilayered nature of the sequences provides evidence of changes in palaeoenvironmental conditions and associated depositional processes. Lithologic and chronological data on the sediments under consideration show that the sequences, as expected, consist mainly of marine and occasionally glaciomarine deposits (Fig. 9). Marine units are correlated not only to the interglacial

https://doi.org/10.1017/qua.2024.24 Published online by Cambridge University Press

epoch but also with periods of significant cooling (Fig. 10). Based on the available research material, the sedimentologic successions from the sections on the southern Kola Peninsula (Figs. 2, 4–7, 9, and 10) are indicative of the Boreal marine transgression, encompassing at least two phases of marine environments (Units 1a and 1b in the Varzuga sections 1(a2) and 1(b3) and in sections 2 [Chavanga], 4 [Chapoma 1], 5N and 5S [Chapoma 2 north and Chapoma 2 south], and 6 [Bolshaya Kumzhevaya] in Fig. 9). The interglacial marine environments also occurred in MIS 3 (Unit 3 in sections 2(b) [Chavanga], 3 [Kamenka], 5N [Chapoma 2 north], 6 [Bolshaya Kumzhevaya] in Fig. 9), covering in the studied sections a shorter time span than the entirety of MIS 3 (Fig. 10), in contrast to the data on the eastern regions of the Eurasian North, where MIS 3 marine sediments are ESR dated on mollusc shells to the interval of ca. 59–25 ka (Molodkov, 2020). Furthermore, the presence of glacial expansion into the coastal areas of the White Sea during early MIS 4 (Unit 2 in the sections 1(b3) and 1(c) [Varzuga], 2(b) [Chavanga], 3 [Kamenka], and 4 [Chapoma 1] in Figs. 9 and 10) and the MIS 3 marine transgressions is observed. According to previous research in the areas adjacent to the Kola Peninsula (Svendsen et al., 2004; Lambeck et al., 2006; Larsen et al., 2006), it is suggested that the BSIS or a local ice sheet may have reached the coastal Kola Peninsula in MIS 4 (see orange line in Fig. 1). Indirect evidence of the BSIS expansion is in the form of pebbles and boulders of exotic rocks that are not known in the bedrock on the Kola region. On the eastern Tersky Coast and adjacent Gorlo Strait shelf, boulders and pebbles of massive and organogenic-detrital carbonate rocks containing abundant fauna of brachiopods, bryozoans, and echinoderms were found in contemporaneous marine deposits (Korsakova et al., 2007; Korsakova, 2021). Occurrence of short-lived marine environments and glacial expansion during the late Valdaian (late Weichselian, MIS 2) glaciation (Unit 4 in the studied sections in Fig. 9) were also demonstrated.

The Varzuga section provides a comprehensive late Pleistocene history from the MIS 5–4 stages. Age determinations reveal marine sediments with ESR and IR-OSL ages ranging from 104.0 ± 8.3 ka to 95.9 ± 11.1 ka, indicating the latter half of the MIS 5 marine environment. The unit in the lowermost part of the Chapoma 1 section indicates an initial phase of the Boreal transgression starting around 138–128 ka, while the following unit in Chapoma 2 section shows its late phase, dated at 72.4 ± 5.6 ka. The lower part of the Bolshaya Kumzhevaya section dates back to 95.9 ± 6.3 ka and is correlated with the middle of the Boreal transgression.

The presence of Unit 2 glacial deposits in the Kamenka sequence (section 3 in Fig. 9) and glacioaqueous deposits in the Chavanga and Chapoma 1 sequences (sections 2 and 4 in Fig. 9) indicates that during the MIS 4 period, the ice sheet covered only the eastern part of the Kola Peninsula. During this time, marine environments predominated in the White Sea depression, with marine and glacial–marine sediments identified and dated to 69–32 ka in the studied sediment successions (sections: 1(c) [Varzuga] 2 [Chavanga], 4 [Chapoma 1], 5N [Chapoma 2 north], 6 [Bolshaya Kumzhevaya] in Fig. 9). Figure 10 illustrates that these sediments correlate not only with the warm MIS 3 but also with the cold MIS 4.

The presence of marine deposits with ages ranging from approximately 37 ka to 59 ka in the Chavanga, Kamenka, Chapoma 1, and Chapoma 2 sections suggests an accumulation stage in the marine environment, encompassing the very end of MIS 4 and almost the entirety of MIS 3. The research material from the studied sections provides evidence of the Boreal marine transgression during MIS 5, a short glacial expansion into coastal areas of the White Sea during early MIS 4, and glaciation in the late MIS 3 and MIS 2 (Fig. 10).

Conclusions

The study of the multilayered sedimentary sequence on the southern coast of the Kola Peninsula provided valuable insights into the dynamics of the palaeoenvironment and accumulation processes for most of the late Pleistocene period.

It was found that the sedimentary sequences are associated with the Boreal marine transgression during MIS 5, characterized by at least two phases of marine environments (Units 1a and 1b). Additionally, the expansion of glaciers into the coastal areas of the White Sea during MIS 4 (Unit 2) and the alternating transgression and regression phases of the sea during MIS 3 (Unit 3) was observed, along with the formation of short-lived marine environments and glacier expansion during the late Valdaian (late Weichselian, MIS 2) glaciation (Unit 4).

Marine environments are correlated not only with the interglacial stages, but also with glacial stages. During MIS 4, the BSIS or a local ice sheet reached the coastal Kola Peninsula and a marine basin continuously existed in the White Sea depression during MIS 5–3 and early MIS 2. The Tersky Coast of the White Sea was glaciated in the late MIS 3–MIS 2.

The results of this study emphasize the significance and complexity of palaeoenvironmental processes on the southern Kola Peninsula and provide new insights for understanding climate changes and glacial events in the late Pleistocene. Overall, our study underscores the importance of an integrated approach to studying sedimentology and palaeoenvironmental conditions for advancing our knowledge of past palaeoenvironmental dynamics. These findings contribute to our understanding of late Pleistocene geologic history and highlight the complex alternation between marine transgressions and glacial expansions and how it affected environmental conditions in the northern European region.

Data availability statement. Data presented in this manuscript are available on request.

Funding. This research was carried out within the framework of the research projects of the Geological Institute of the Kola Science Centre, Russian Academy of Sciences FMEZ-2024-0007 and Institute of Geography, Russian Academy of Sciences FMWS-2024-0003 and partly (dating samples) supported by RSF grant 22-17-00081.

Competing interests. The authors state they have no known competing financial interests or personal relationships that could have appeared to influence the work described in this paper.

References

Adamiec, G., Aitken, M., 1998. Dose-rate conversion factors: update. *Ancient TL* **16**, 37–50.

Apukhtin, N.I., 1957. Stratigraphy of Quaternary deposits of the Kola Peninsula and North Karelia according to new research. In: *Proceedings for the Geology and Commercial Minerals of the North-Western USSR*. Vol. 1. [In Russian.] Gosgeoltekhizdat, Leningrad, pp. 68–83.

Apukhtin, N.I., 1978. New data on the stratigraphy of Quaternary sediments of the southern part of the Kola Peninsula. [In Russian.] *Transactions of the All-Russian Geological Institute: Quaternary Geology and Geomorphology* **297**, 53–65.

https://doi.org/10.1017/qua.2024.24 Published online by Cambridge University Press

Armand, A.D., Armand, N.N., Grave, M.K., Yevzerov, V.Ya., Lebedeva, R.M., 1969. Generalized scheme of Quaternary (Anthropogen) deposits of the Kola Peninsula in the light of the new data. In: Grave, M.K., Koshechkin, B.I. (Eds.), *Main Problems of Geomorphology and Anthropogen Stratigraphy of the Kola Peninsula*. [In Russian.] Nauka Press, Leningrad, pp. 7–24.

Armand, A.D., Lebedeva, R.M., 1966. Spore-and-pollen characteristic of the key section of interglacial deposits in the southern coastal area of Kola Peninsula. In: Grave, M.K., Armand, F.L. (Eds.), *Formation of the Relief and Quaternary Deposits of the Kola Peninsula*. [In Russian.] Nauka Press, Moscow-Leningrad, pp. 77–86.

Arslanov, Kh.A., Yevzerov, V.Ya., Tertychnyy, N.I., Gerasimov, S.A., Lokshin, N.V., 1981. On the age of deposits (Ponoy Beds) Boreal transgression in the Kola Peninsula. In: Velichko, A.A., Faustova, M.A. (Eds.), *Pleistocene Glaciations on the East European Plain*. [In Russian.] Nauka Press, Moscow, pp. 28–37.

Astafiev, B.Yu., Bogdanov, Yu.B., Voinova, O.A., Zhuravlev, V.A., Nogina, M.Yu., Paramonova, M.S., Peshkova, I.N., *et al.*, 2012. *National Map of the Russian Federation. 1:1 000 000 (third generation). Baltic Series, Sheet Q-37–Arkhangelsk. Explanatory Note*. [In Russian.] All-Russian Geological Institute (VSEGEI) Press, St. Petersburg. https://vsegei.ru/ru/info/pub_ggk1000-3/Baltiyskaya/q-37.php, accessed May 15, 2023.

Ayling B., Eggins S., McCulloch M., Chappell J., Grün R, Mortimer G., 2017. Uranium uptake history, open-system behaviour and uranium-series ages of fossil *Tridacna gigas* from Huon Peninsula, Papua New Guinea. *Geochimica et Cosmochimica Acta* **213**, 475–501.

Bolikhovskaya, N., Molodkov, A., 2007. Pollen and IR-OSL evidences for palaeoenvironmental changes between ca. 39 kyr to ca. 33 kyr BP recorded in the Voka key section, NE Estonia. In: Johansson, P., Sarala, P. (Eds.), *Applied Quaternary Research in the Central Part of Glaciated Terrain*. Vol. 46. Geological Survey of Finland, Special Paper, pp. 103–112.

Boyes, B.M, Linch, L.D., Pearce, D.M., Kolka, V.V., Nash, D.J., 2021.The Kola Peninsula and Russian Lapland: a review of Late Weichselian glaciation. *Quaternary Science Reviews* **267**, 1–28.

Boyes, B.M., Linch L.D., Pearce, D.M., Nash, D.J., 2023. The last Fennoscandian Ice Sheet glaciation on the Kola Peninsula and Russian Lapland (Part 2): ice sheet margin positions, evolution, and dynamics. *Quaternary Science Reviews* **300**, 107872.

Cheremisinova, E.A., 1962. Diatom flora of marine interglacial deposits on the Kola Peninsula. In: *Proceedings for the Geology and Commercial Minerals of the North-Western RSFSR*, Vol. 3. [In Russian.] Nauka Press, Leningrad, pp. 45–57.

Choukri, A., Hakam, O.-K., Reyss, J.-L., Plaziat, J.-C., 2007. Radiochemical dates obtained by alpha spectrometry on fossil mollusk shell from the 5e Atlantic shoreline of the High Atlas, Morocco. *Applied Radiation and Isotopes* **65**, 883–890.

Demidov, I.N., Houmark-Nielsen, M., Kjær, K.H., Larsen, E., 2006. The last Scandinavian Ice Sheet in northwestern Russia: ice flow patterns and decay dynamics. *Boreas* **35**, 425–443.

Ekman, I., Iljin, V., 1991. *Deglaciation, the Younger Dryas End Moraines and Their Correlation in the Karelian A.S.S.R and Adjacent Areas*. Geological Survey of Finland, Espoo.

Farr, T.G., Rosen, P.A., Caro, E., Crippen, R., Duren, R., Hensley, S., Kobrick, M., *et al.*, 2007. The Shuttle Radar Topography Mission. *Reviews of Geophysics* **45**, 1944-9208.

Faustova, M.A., 1984. Late Pleistocene glaciation of European USSR. In: Velichko, A.A. (Ed.), *Late Quaternary Environments of the Soviet Union*. University of Minnesota Press, Minneapolis, pp. 3–12.

Funder, S., Demidov, I., Yelovicheva, Ya., 2002. Hydrography and mollusc faunas of the Baltic and the White Sea-North Sea seaway in the Eemian. *Palaeogeography, Palaeoclimatology, Palaeoecology* **184**, 275–304.

Godfrey-Smith D.I., Huntley, D.J., Chen, W.H., 1988. Optical dating studies of quartz and field-spar sediment extracts. *Quaternary Science Reviews* **7**, 373–380.

Grave, M.K., Gunova, V.S., Devyatova, E.I., Lavrova, M.A., Lebedeva, R.M., Samsonova, L.Ya., Cheremisinova, E.A., 1969. Mikulinskoye mezhledni-koviye na yugo-vostoke Kolskogo poluostrova [Mikulino interglacial in the South-East of the Kola Peninsula]. In: Grave, M.K., Koshechkin, B.I. (Eds), *Main problems of Geomorphology and Anthropogen Stratigraphy of the Kola Peninsula*. [In Russian.] Nauka Press, Leningrad, pp. 25–56.

Grøsfjeld, K., Funder, S., Seidenkratz, M.-S., Glaister, C., 2006. Last Interglacial marine environments in the White Sea region, northwestern Russia. *Boreas* **35**, 493–520.

Grosswald, M.G., 2001. The Late Weichselian Barents-Kara ice sheet: in defense of a maximum reconstruction. *Russian Journal of Earth Sciences* **3**, 427–452.

Grosswald, M.G., Hughes, T.J., 2002. The Russian component of an Arctic ice sheet during the Last Glacial Maximum. *Quaternary Science Reviews* **21**, 121–146.

Gudina, V.I., Yevzerov, V.Ya., 1973. Review of *The Stratigraphy and Foraminifera of the Upper Pleistocene in the Kola Peninsula*. Originally published in Russian (Transaction of the Institute of Geology and Geophysics, Kola Branch of the Academy of Sciences of the USSR, issue 175). Translated by Dr E. Lees, and issued by the British Library. *Geological Magazine* **119**(3).

Gusev, E.A., Molodkov, A.N., 2012. Structure of sediments of the final stage of the Kazantsevo transgression (MIS 5) in the north of western Siberia. *Doklady Earth Sciences* **443**, 458–461.

Gusev, E.A., Molodkov, A.N., Streletskaya, I.D., Vasiliev, A.A., Anikina, N.Y., Bondarenko, S.A., Derevyanko, L.G., *et al.*, 2016. Deposits of the Kazantsevo transgression (MIS 5) in the northern Yenisei region. *Russian Geology and Geophysics* **57**, 586–596.

Hättestrand, C., Clark, Ch.D., 2006. The glacial geomorphology of Kola Peninsula and adjacent areas in the Murmansk Region, Russia. *Journal of Maps* **2**(1), 30–42.

Hättestrand, C., Kolka, V.V., Stroeven, A.P., 2007. The Keiva ice marginal zone on the Kola Peninsula, northwest Russia: a key component for reconstructing the palaeoglaciology of the northeastern Fennoscandian Ice Sheet. *Boreas* **36**, 352–370.

Hughes, A.L.C., Gyllencreutz, R., Lohne, O.S., Mangerud, J., Svendsen, J.I., 2016. The last Eurasian ice sheets—a chronological database and time-slice reconstruction, DATED-1. *Boreas* **45**, 1–45.

Huntley, D.J., Baril, M.R., 1997. The K content of K-feldspars being measuring in optical dating or in thermoluminescence dating. *Ancient TL* **15**, 11–13.

Huntley, D.J., Godfrey-Smith, D.I., Thewalt, M.L.W., 1985. Optical dating of sediments. *Nature* **313**, 105–107.

Huntley, D.J., Hancock, R.G.V., 2001. The Rb contents of the K-feldspar grains being measured in optical dating. *Ancient TL* **19**, 43–46.

Ikonen, L., Ekman, I., 2001. Biostratigraphy of the Mikulino interglacial sediments in NW Russia: the Petrozavodsk site and a literature review. *Annales Academiae Scientiarum Fennicae, series A, III, Geologica-geographica* **161**, 1–88.

Jaek, I., Molodkov, A., Vasilchenko, V., 2008. Instability of luminescence responses in feldspar- and quartz-based palaeodosimeters. *Journal of Applied Spectroscopy* **75**, 820–825.

Jaek, I., Molodkov, A., Vasilchenko, V., 2010. The mechanisms of luminescence response to optical and thermal stimulation of alkali feldspars. *Journal of Applied Spectroscopy* **77**, 441–444.

Kaufman, A., Broecker, W.S., 1965. Comparison of ^{230}Th and ^{14}C ages for carbonates materials from Lakes Lahontan and Bonneville. *Journal of Geophysical Research* **70**, 4039–4054.

Kaufman, A., Chaleb, B., Wehmiller, J., Hillaire-Marsel, C., 1996. Uranium concentration and isotope ratio profiles within Mercenariu shells: geochronological implications. *Geochimica et Cosmochimica Acta* **60**, 3735–3746.

Kind, N.V., 1974. *Anthropogen Geochronology Based on Isotope Data*. [In Russian.] Nauka Press, Moscow.

Kjær, K.H., Larsen, E., Funder, S., Demidov, I.N., Jensen, M., Hekansson, L., Murray, A., 2006. Eurasian ice-sheet interaction in northwestern Russia throughout the Late Quaternary. *Boreas* **35**, 444–475.

Kleman, J., Hättestrand, C., Borgström, I., Stroeven, A.P., 1997. Fennoscandian palaeoglaciology reconstructed using a glacial geological inversion model. *Journal of Glaciology* **43**, 283–299.

Kolka, V.V., Korsakova, O.P., 2017. The position of the coastal line of the White Sea and neotectonic movements in the north-east of Fennoscandia in the late glacial and Holocene. In: Lisitsin, A.P. (Ed.), *The White Sea*

https://doi.org/10.1017/qua.2024.24 Published online by Cambridge University Press

System. Vol. IV, *The Processes of Sedimentation, Geology and History*. [In Russian.] Scientific World Press, Moscow, pp. 222–249.

Korsakova, O., 2019. Formal stratigraphy of the Neopleistocene (Middle and Upper/Late Pleistocene) in the Kola region, NW Russia. *Quaternary International* **534**, 42–59.

Korsakova, O., 2021. Upper Pleistocene and Holocene stratigraphy in the Kola Peninsula and Northern Karelia (N–W Russia): marine and glacial units. *Quaternary International* **605–606**, 108–125.

Korsakova, O., Kolka, V., Semenova, L., 2016. Late Pleistocene stratigraphy according to the sediment sequence from eastern Kola Peninsula, Ponoi River Valley (north-western Russia). *Quaternary International* **420**, 280–293.

Korsakova, O., Molodkov, A., Yelovicheva, Ya., Kolka, V., 2019. Middle Pleistocene marine deposits on the Kola Peninsula (NW Russia). *Quaternary International* **509**, 3–16.

Korsakova, O., Vashkov, A., Nosova, O., 2021. European Russia: glacial landforms from the Last Glacial Maximum. In: Palacio, D., Hughes, Ph.D., Garcia-Ruiz, J.M., Andres, N. (Eds.), *European Glacial Landscapes. Maximum Extent of Glaciation*. Elsevier, Amsterdam, pp. 389–394.

Korsakova, O.P., Kolka, V.V., Zozulya, D.R., 2007. On a possible ingression of the late Pleistocene Kara Ice Sheet to the Kola Peninsula. In: Lavrushin, Yu.A., Khoreva, I.M., Chistyakova, I.A. (Eds.), *Fundamental Issues of the Quaternary, Results of Study and the Main Trends of Further Research: Proceeding of the V All-Russian Conference on Quaternary Research*. [In Russian.] GEOS Press, Moscow, pp. 193–195.

Korsakova, O.P., Molodkov, A.N., Kolka, V.V., 2004. Geological-stratigraphic position of Upper Pleistocene marine sediments in the southern Kola Peninsula: evidence from geochronological and geological data. *Doklady of Earth Sciences* **398**, 908–912; translation, *Doklady Akademii Nauk* 398, 218–222.

Koshechkin, B.I., 1979. *Holocene Tectonics of the Eastern Part of the Baltic Shield*. [In Russian.] Nauka Press, Leningrad.

Labonne, M., Hillaire-Marcel, C., 2000. Geochemical gradients within modern and fossil shells of *Concholepas concholepas* from northern Chile: an insight into U-Th systematics and diagenetic/authigenic isotopic imprints in mollusk shells. *Geochimica et Cosmochimica Acta* **64**, 1523–1534.

Lambeck, K., Purcell, A., Funder, S., Kjær, K.H., Larsen, E., Möller, P., 2006. Constraints on the Late Saalian to early Middle Weichselian ice sheet of Eurasia from field data and rebound modelling. *Boreas* **35**, 539–575.

Lambeck, K., Purcell, A., Zhao, J., Svenson, N.-O., 2010. The Scandinavian Ice Sheet: from MIS 4 to the end of the Last Glacial Maximum. *Boreas* **39**, 410–435.

Larsen, E., Kjær, K.H., Demidov, I.N., Funder, S., Grosfjeld, K., Houmark-Nielsen, M., Linge, H., Lysså, A., 2006. Late Pleistocene glacial and lake history of northwestern Russia. *Boreas* **35**, 394–424.

Lavrova, M.A., 1960. *Quaternary Geology of the Kola Peninsula*. [In Russian.] Academia Science Press, Moscow-Leningrad.

Lunkka, J.P., Kaparulina, E., Putkinen, N., Saarnisto, M., 2018. Late Pleistocene palaeoenvironments and the last deglaciation on the Kola peninsula, Russia. *Arktos* **4**, 1–18.

Maksimov, F.E., Sharin, V.V., Kuznetsov, V.Yu., Okunev, A.S., Grigoriev, V.A., Petrov, A.Yu., 2016. Uranium-thorium dating of high sea terraces of the Spitsbergen Archipelago. *Vestnik of Saint-Petersburg University, series 7, Geology, Geography* **2**, 54–64.

Malyasova, E.S., 1960. Application of the spore-pollen method for stratigraphic subdivision of the Quaternary deposits of the Kola Peninsula and the Karelian Isthmus. In: Pokrovskaya, I.M. (Ed.), *Collected articles on paleogeography and stratigraphy of Quaternary deposits*. Iss. 2. [In Russian.] LGY Press, Leningrad, pp. 26–38.

Miller, G.H., Mangerud, J., 1985. Aminostratigraphy of European marine interglacial deposits. *Quaternary Science Reviews* **4**, 215–278.

Mitrofanov, F.P. (Ed.), 2001. Geological Map of the Kola Region. 1:1500,000. GI KSC RAS, Apatity. https://www.geokniga.org/maps/545, accessed November 14, 2023.

Molodkov, A., 2012. Cross-check of the dating results obtained by ESR and IR-OSL methods: implication for the Pleistocene palaeoenvironmental reconstructions. *Quaternary Geochronology* **10**, 188–194.

Molodkov, A., 2020. The Late Pleistocene palaeoenvironmental evolution in northern Eurasia through the prism of the mollusc shell-based ESR dating evidence. *Quaternary International* **556**, 180–197.

Molodkov, A., Bitinas A., 2006. Sedimentary record and luminescence chronology of the Lateglacial and Holocene Aeolian sediments in Lithuania. *Boreas* **35**, 244–254.

Molodkov, A., Bolikhovskaya, N., 2002. Eustatic sea-level and climate changes over the last 600 ka as derived from mollusc-based ESR-chronostratigraphy and pollen evidence in northern Eurasia. *Sedimentary Geology* **150**, 185–201.

Molodkov, A., Bolikhovskaya, N., 2009. Climate change dynamics in northern Eurasia over the last 200 ka: evidence from mollusc-based ESR-chronostratigraphy and vegetation successions of the loess–palaeosol records. *Quaternary International* **201**, 67–76.

Molodkov, A., Bolikhovskaya, N., 2010. Climato-chronostratigraphic framework of Pleistocene terrestrial and marine deposits of northern Eurasia based on pollen, electron spin resonance, and infrared optically stimulated luminescence analyses. *Estonian Journal of Earth Sciences* **59**, 49–62.

Molodkov, A., Jaek, I., Vasilchenko, V., 2007. Anomalous fading of IR-stimulated luminescence from feldspar minerals: some results of the study. *Geochronometria* **26**, 11–17.

Molodkov, A., Raukas, A., 1998. ESR age of the Late Pleistocene transgressions in the eastern part of the White Sea coast. *Geologija* (*Vilnius*) **25**, 62–69.

Molodkov, A., Yevzerov, V., 2004. ESR/OSL ages of long-debated subtill fossil-bearing marine deposits from the southern Kola Peninsula: stratigraphic implications. *Boreas* **33**, 123–131.

Nikonov, A.A., 1966. Anthropogen stratigraphy and paleogeography of the Kola Peninsula and adjacent areas. In: Grichuk, V.P. (Ed.), *Upper Pleistocene: Stratigraphy and Absolute Geochronology*. [In Russian with English abstract.] Nauka Press, Moscow, pp. 92–105.

Nikonov, A.A., Vostrukhina, T.M., 1964. On the Anthropogen stratigraphy in the North-Eastern Kola Peninsula. [In Russian.] *Doklady Akademii Nauk USSR* **158**, 104–107.

Pasanen, A., Lunkka, J.P., Putkinen, N., 2010. Reconstruction of the White Sea basin during the late Younger Dryas. *Boreas* **39**, 273–285.

Prescott, J.R., Hutton, J.T., 1994 Cosmic ray contributions to dose rates for luminescence and ESR dating: large depths and long-term time variations. *Radiation Measurement* **23**, 497–500.

Rippas, P.B., 1899. The Kola Expedition of 1898 (preliminary report). [In Russian.] *Proceedings of the Imperial Russian Geographical Society* **35**, 292–312.

Rowe, P.J., Turner, J.A., Andrews, J.E., Leeder, M.R., Calsteren, P. van, Thomas, L., 2015. Uranium-thorium dating potential of the marine bivalve *Lithophaga lithophaga*. *Quaternary Geochronology* **30**, 80–89.

Strelkov, S.A., Yevzerov, V.Ya., Koshechkin, B.I., Rubinraut, G.S., Afanasiev, A.P., Lebedeva, R.M., Kagan, L.Ya., 1976. *The History of the Formation of Relief and Loose Sediments in the Northeastern Part of the Baltic Shield*. [In Russian.] Nauka Press, Leningrad.

Stroeven, A.P., Hättestrand, C., Kleman, J., Heyman, J., Fabel, D., Fredin, O., Goodfellow, B.W., *et al.*, 2016. Deglaciation of Fennoscandia. *Quaternary Science Reviews* **147**, 91–121.

Svendsen, J.I., Alexanderson, H., Astakhov, V.I., Demidov, I.N., Dowdeswell, J.A., Funder, S., Gataullin, V., *et al.*, 2004. Late Quaternary ice sheet history of Northern Eurasia. *Quaternary Science Reviews* **23**, 1229–1271.

Vasilchenko, V., Molodkov, A., Jaek, I., 2005. Tunnel processes and anomalous fading in natural feldspars extracted from Quaternary deposits. *Journal of Applied Spectroscopy* **72**, 218–223.

Wallinga, J., Murray, A. S., Duller, G.A.T., Tornqvist, T.E., 2001. Testing optically stimulated luminescence dating of sand-sized quartz and feldspar from fluvial deposits. *Earth and Planetary Science Letters* **193**, 617–630.

Yevzerov, V.Ya. (Ed.), 1993. *Eastern Fennoscandian Younger Dryas End Moraines and Deglaciation. Excursion Guide, Field Conference on Termination of the Pleistocene—IGCP Project 253, July, 15–21, Kola Peninsula*. Geological Institute of the Kola Science Centre of the Russian Academy of Sciences, Apatity.

https://doi.org/10.1017/qua.2024.24 Published online by Cambridge University Press

Yevzerov, V.Ya., 2001. Valdai (Weichselian) glaciation in the Kola region. In: Matishov, G.G., Denisov, V.V., Dzhenyuk, S.L., Tarasov, G.A. (Eds.), *Problems and Methods of Ecological Monitoring of the Seas and Coastal Zones of the Western Arctic Regions*. [In Russian.] Kola Science Centre, Apatity, pp. 20–33.

Yevzerov, V.Ya., 2016. *Geology of the Quaternary Deposits of the Kola Region*. [In Russian.] Murmansk State Technical University Press, Murmansk.

Yevzerov, V.Ya., Yelovicheva, Ya.K., Lebedeva, R.M., Rayamyae, R.A., 1981. Stratigraphy of Pleistocene deposits in the southern part of the Kola Peninsula. In: Evzerov, V.Ya. (Ed.), *Geology of the Pleistocene of the North-West of the USSR*. [In Russian.] Kola Branch of the USSR Academy of Sciences, Apatity, pp. 97–107.

Zaretskaya, N., Korsakova, O., Molodkov, A., Ruchkin, M., Baranov, D., Rybalko, A., Lugovoy, N., Merkuliev, A., 2022. Early Middle Weichselian in the White Sea and adjacent areas: chronology, stratigraphy and palaeoenvironments. *Quaternary International* **632**, 65–78.

Zaretskaya, N.E., Korsakova, O.P., Panin, A.V., 2019. Marine Isotopic Stage 3 in Northeastern Europe: geochronology and events. *Russian Geology and Geophysics* **60**, 911–925.

Zarkhidze, D.V., Gusev, E.A., Anikina, N.Yu., Bartova, A.V., Gladenkov, A.Yu., Derevianko, L.G., Krylov, A.V., Tverskaya, L.A., 2010. New data on stratigraphy of the Pliocene-Quaternary deposits in the More-Yu River basin (Bolshezemelskaya tundra). [In Russian.] *Geological and Geophysical Characteristics of the Lithosphere of the Arctic Region* **7**, 96–110.

Zatsepin, V.I., Filatova, Z.A., 1961. The bivalve mollusc *Cyprina islandica* (L.), its geographic distribution and role in the communities of benthic fauna. [In Russian.] *Transactions of Institute of Oceanology of USSR Academy of Sciences* **46**, 201–216.

https://doi.org/10.1017/qua.2024.24 Published online by Cambridge University Press